Geochemistry

Wabamun Area CO$_2$ Sequestration Project (WASP)

Authors

Maurice Shevalier

Michael Nightingale

Bernhard Mayer

Rev.	Date	Description	Prepared by
1	January 4, 2010	Geochemical Analysis of WASP Study Area	Dr. Bernhard Mayer

Table of Contents

List of Tables

INTRODUCTION

Carbon capture and storage (CCS) is a promising approach for reducing anthropogenic CO_2 emissions to the atmosphere as a means of mitigating future impacts of human-induced climate change *[1]*. Successful CCS projects should demonstrate that the injected CO_2 is safely and securely sequestered in the chosen reservoir. It is not only important to demonstrate that CO_2 has been stored, but also desirable to evaluate how much CO_2 is sequestered in soluble, ionic or mineral form. Geochemical monitoring programs are an excellent tool for tracing the movement and the fate of the injected CO_2 in the reservoir and to assess the nature and effectiveness of the storage mechanisms *[e.g., 2]*.

The injected CO_2 first dissolves in the water to become an aqueous species, i.e., $CO_{2(aq)}$. Once in this form the $CO_{2(aq)}$ can undergo a number of reactions with the fluids and minerals present in the reservoir. These include:

1. reaction with the formation water *[3]*;
2. reaction with carbonate minerals present in the reservoir *[3]*;
3. reaction with carbonate and silicate minerals present in the reservoir *[4]*.

In the first reaction, $CO_{2(aq)}$ will react with water as follows *[3]*:

$$CO_{2(aq)} + H_2O \leftrightarrow H_2CO_3 \qquad \text{(i)}$$
$$H_2CO_3 \leftrightarrow H^+ + HCO_3^- \qquad \text{(ii)}$$

This trapping of $CO_{2(aq)}$, **solubility trapping**, will result in changes of geochemical parameters that can be monitored, i.e., there will be a decrease in the pH of the water due to the disassociation of H_2CO_3 and changes in the isotopic composition of the HCO_3^- dependant on the isotopic composition of the injected CO_2.

In the second reaction, the carbonic acid reacts with carbonate minerals that may be present in the reservoir as shown below *[3]*:

$$CO_{2(aq)} + H_2O \leftrightarrow H_2CO_3 \qquad \text{(iii)}$$
$$H_2CO_3 \leftrightarrow H^+ + HCO_3^- \qquad \text{(iv)}$$
$$H^+ + CaCO_3 \rightarrow Ca^{2+} + HCO_3^- \qquad \text{(v)}$$
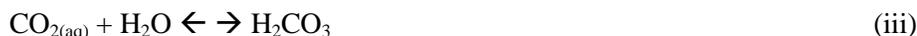
The net reaction is as follows:

$$H_2O + CO_{2(aq)} + CaCO_3 \rightarrow Ca^{2+} + 2HCO_3^- \qquad \text{(vi)}$$

In this reaction sequence a carbonate mineral, such as calcite, reacts with the carbonic acid, which is formed by the dissolution of $CO_{2(aq)}$ in water resulting in the formation of two moles of HCO_3^- for each mole of $CO_{2(aq)}$. This is known as **ionic trapping** and is a very stable and secure form of storage since the $CO_{2(aq)}$ is now in trapped as a dissolved species in solution. This reaction results in an increase in the concentrations of Ca^{2+} and HCO_3^-, which can be monitored geochemically. Further, there will be changes in the carbon isotope ratio of HCO_3^-. These changes will be governed not only by the isotopic composition of the injected CO_2 but also by the isotopic composition of the carbonate minerals.

The third reaction involves $CO_{2(aq)}$ reacting with both carbonate and silicate minerals which may be present in the reservoir, as shown below *[4]*:

$$CaAl_2Si_2O_8 + CO_{2(aq)} + 2H_2O \rightarrow CaCO_3 + Al_2Si_2O_5(OH)_4 \qquad (vii)$$

anorthite   calcite   kaolinite
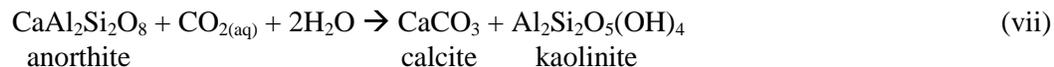
In this reaction, $CO_{2(aq)}$ reacts with a silicate mineral, in this case anorthite, to form calcite. Here the $CO_{2(aq)}$ is trapped as a solid phase, i.e., **mineral trapping**, in this case calcite. Mineral trapping achieves long term stable and secure storage of $CO_{2(aq)}$.

In the Wabamun Area Sequestration Project (WASP), the goal of the Applied Geochemistry Group (AGg) was to assess and predict the potential extent of solubility, ionic and mineral trapping of $CO_{2(aq)}$ in the Nisku aquifer. This was achieved by geochemical characterization of reservoir fluids using geochemical and isotopic techniques, mineralogical analyses on reservoir and caprock core material, and reactive transport modelling. The latter modelled different geochemical reactions occurring in the reservoir.

DISCUSSION

1.   BASELINE GEOCHEMISTRY OF NISKU FLUIDS AND GASES: CHEMICAL AND ISOTOPIC COMPOSITION

To reach the goals of this project it was important to obtain an understanding of the regional geochemistry of the formation waters and gases and hence to determine a geochemical baseline prior to potential CO_2 injection into the Nisku aquifer.

1.1   Data Sources

The WASP study area is shown in Figure 1. Chemical and isotopic data for formation waters as well as gas composition and gas isotope data for this area have been obtained from a number of sources in order to determine the baseline geochemistry. The data sources include the Energy Resources Conservation Board (ERCB) data base, the Ph.D. thesis of Graham Simpson entitled "Sulfate reduction and fluid chemistry of the Devonian Leduc and Nisku formations in south-central Alberta" *[5]*, and our own analyses of fluids and gases obtained from a water source well producing from the Nisku formation.
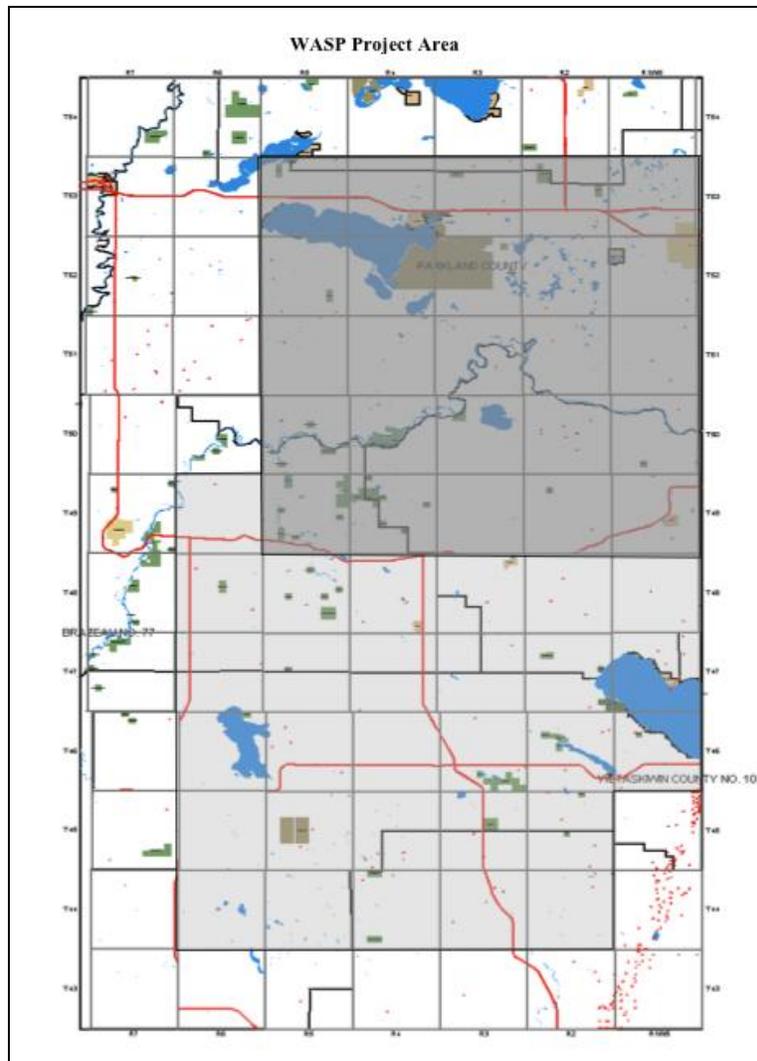
Figure 1: Study area of the WASP project located in central Alberta.

The chemical data available for the Nisku formation waters from the ERCB data base are subject to a number of potential inaccuracies and inaccurate analyses must be identified and removed *[6]*. Contamination associated with drilling, completion and production methods, incorrect sampled intervals, multiple tested intervals, data entry errors, and multiple entries are the most common forms of error. The following culling methods are modified from those described by Bachu et al. *[6]*. Data entries with analyses missing any of the major ions Na, Cl, Ca and alkalinity, were ignored, as well as those collected from production locations down-stream of the separators (facilities where water-oil or water-gas mixtures are separated). Waters with densities less than 1, pH less than 4 or greater than 10, and those with lab analysis dates more than 1 month after sample collection dates were also culled. Data entry errors were identified by calculating charge balances, with imbalances of greater than 5% being culled. Contamination by drilling mud, acid washes or washes from cement jobs were determined by cross-plotting the various cations and anions and by reviewing the recovery descriptions. Duplicate analyses, and analyses from larger test intervals, multiple intervals, and incorrect intervals were removed by scrutinizing the individual well samples.

The remaining geochemical analyses were used to map the distribution of water chemistry that is considered to be representative of the Nisku aquifer. There were 40 wells in the ERCB data base within the WASP study area that had pH values and major ion geochemistry for the reservoir fluids that were considered representative for the Nisku formation. Table 1 summarizes the available chemical parameters for Nisku fluids from these 40 wells.

The ERCB data base does not contain any data on the isotopic composition of reservoir fluids. The Ph.D. thesis of Graham Simpson *[5]* completed at the University of Calgary in 1999 summarizes information on the isotopic composition of fluids and dissolved constituents in the Nisku Formation. None of the samples described in *[5]* were obtained from within the WASP study area. However, since this thesis contains the only known source of high quality isotopic data from the Nisku formation it was viewed as important to review the isotopic composition of Nisku fluids in the surroundings of the WASP study area. A total of 33 wells from the thesis were used in this study. Table 2 lists the wells and summarizes the isotopic composition of water (δ^2H, δ^{18}O), sulfate (δ^{34}S-SO$_4$), sulfide (δ^{34}S-S^{2-}) and dissolved inorganic carbon (δ^{13}C-HCO$_3$).

Table 1: pH, total dissolved solids, and major ion concentrations for fluids in the Nisku Formation obtained from the ERCB data base.

Location	pH	Sodium (mg/L)	Calcium (mg/L)	Magnesium (mg/L)	Chloride (mg/L)	Bicarbonate (mg/L)	Sulfate (mg/L)	TDS Calculated (mg/L)
10-08-044-01W5	7.6	38538	7581	1314	75164	130	1969	124696
07-31-044-04W5	6.8	43976	16657	1798	101250	732	1187	165600
07-31-044-04W5	7.3	48254	16235	1712	106832	254	1141	208610
10-33-044-04W5	6.5	57592	17778	1968	124750	771	1132	203991
10-33-044-04W5	6.5	53936	17017	2065	118625	762	355	192760
15-11-045-01W5	7.5	57064	12835	2114	116232	110	765	189120
05-23-045-01W5	7.4	36701	7384	1025	70430	595	2530	118665
11-24-045-01W5	7.9	56694	11956	2313	114724	180	708	186575
11-24-045-01W5	6.5	55704	12852	3206	117242	465	678	190147
14-21-045-02W5	7.1	38983	10699	1452	82000	255	1560	134949
06-05-045-04W5	6.6	52281	14695	1968	110705	880	1585	182114
16-06-045-04W5	6.6	54368	16536	2248	118400	844	1068	193464
16-06-045-04W5	7.7	42505	12472	2770	93000	1050	2848	154645
16-06-045-04W5	6.6	42712	12412	1409	88900	1296	3124	149853
16-06-045-04W5	6.1	55032	19499	2649	126250	759	574	204763
07-08-045-04W5	7.3	61617	17257	2479	132400	602	80	214435
04-22-045-05W5	7.4	8080	2030	344	14233	1510	2642	28839
04-22-045-05W5	6	56860	19092	2910	129250	702	430	209244
10-36-045-05W5	7.4	57397	17448	1723	122823	458	1214	201963
10-25-046-02W5	7.3	49136	14104	1461	103574	532	1188	170476
16-12-046-03W5		57800	15030	200	115060	940	940	190270
05-12-046-05W5	8.2	27504	7399	1061	55200	522	4214	95900
06-19-046-05W5	6.8	43121	16720	2772	102000	330	2701	167644
04-36-047-03W5	7.4	21647	7339	1005	48833	115	535	79474
02-06-047-04W5	9.2	44155	14832	1876	98011	166	1451	161012
02-28-048-02W5	6.6	27378	8332		56272	550	500	93032
02-28-048-02W5	7.3	45309	11089		88830	500	500	146228
14-12-048-06W5	6.2	43600	11430	2768	102000	498	634	163383
15-11-049-02W5	7.2	42000	8610	870	81500	456	1021	134457
15-11-049-02W5	6.7	35400	8260	708	70300	525	808	116001
15-11-049-02W5	7.2	42000	8610	870	81500	456	1021	134457
02-29-051-05W5	6.2	39000	7940	1580	84700	717	604	136453
09-13-052-01W5	7.4	36645	8534	1873	76247	216	948	124463
10-05-052-02W5	5.9	47218	10250	2255	96600	600	785	157708
10-14-053-03W5	6.2	46138	11340	1417	95014	513	24	154446
07-33-053-03W5	6.7	43493	7928	2168	86850	366	487	141292
07-33-053-03W5	6.8	41102	8834	2168	83955	497	1481	138037
13-36-053-03W5	7.5	45018	10890	2193	94200	361	942	153604

Table 2: Isotopic composition of water, sulfate, dissolved sulfide, and dissolved inorganic carbon in samples from the Nisku Formation surrounding the WASP study area; data from *[5]*.

Location	$\delta^{18}O$ in H_2O (‰)	δ^2H in H_2O (‰)	$\delta^{34}S$ in SO_4 (‰)	$\delta^{34}S$ in S^{2-} (‰)	$\delta^{13}C$ in HCO_3 (‰)
15-6-40-23W4	7.8	-55	21.9	16.4	-7.1
10-31-39-23W4	6.5	-52	21.6	20.2	-2.7
12-9-41-23W4	8.2	-43	23.0	19.5	-10.1
13-9-41-23W4	7.5	-49	22.5	19.1	-9.0
8-35-48-12W5	-13.6	-133	22.9		0.9
5-1-40-24W4	3.3	-65	22.9	15.3	-4.3
14-32-13-16W4	-8.8	-88	25.0	16.1	-2.9
14-19-15-16W4	-9.6	-93	24.7	12.5	-8.3
16-4-14-16W4	-9.3	-99	27.7	23.5	-2.4
7-10-56-24W4	-3.9	-81	45.4	18.7	-6.0
16-10-56-24W4	-4.8	-80	48.5	20.4	
16-3-56-24W4	-4.7	-78	47.9	19.4	-6.8
4-10-56-24W4	-4.0	-72	45.9	20.7	-6.9
4-21-57-24W4	-5.1	-84	46.0	15.7	-6.4
2-23-36-20W4	-4.4	-75	24.2	14.7	
11-23-35-20W4	-4.4	-83	23.6	13.2	-7.0
13-3-35-20W4	-4.1	-76	22.5	14.5	-7.5
2-27-37-20W4	-3.5	-71	23.6	13.4	-3.9
9-11-36-20W4	-3.9	-79	25.8		-4.8
16-16-41-2W5	5.1	-48	22.5	16.0	-2.1
10-15-38-24W4	7.6	-50	21.2	18.4	-5.1
12-23-38-24W4	6.0	-54	21.1	16.4	-9.7
3-14-38-24W4	8.1	-54	21.5	19.9	-3.4
10-14-38-24W4	9.3	-53	24.0	18.6	-5.0
7-5-31-27W4	8.8	-49	25.8	17.5	-4.3
5-32-36-21W4	2.5		22.6		-9.6
10-15-29-11W4	1.5	-65	23.5	18.4	-9.2
6-11-29-24W4	0.9	-66	23.3	16.4	
10-14-29-24W4	7.2	-46	22.7	15.0	-15.9
6-9-34-26W4	0.9		24.7	24.8	-12.1
14-27-33-26W4	1.3		27.2	27.4	-13.2
12-11-49-12W5	-13.9	-129	22.7		0.5
4-21-42-23W4	6.6	-56	24.6	15.3	-7.7

Another source of data was from water and gas samples collected from the only known water well completed in the Nisku formation in the study area in 2003 and 2004 (well 100/11-29-045-02W5). These samples were collected when the well first went into production and compositional data were determined by commercial laboratories. The chemical compositions of gases and fluids are summarized in Table 3.

Table 3: Water and gas compositional data for samples from well 100/11-29-045-02W5. Data provided by Conoco-Phillips.

Description	03/01/25	03/01/27	03/06/03	03/08/29	04/12/13	08/06/19	08/09/10
CO_2 (mole %)	0.09	0.05	4.41	5.89	3.07	5.00	
H_2S (mole %)	0.60	0.60	29.23	49.26	8.80	36.01	
N_2 (mole %)	97.08	97.46	2.57	1.51	3.92	1.31	
CH_4 (mole %)	0.36	0.24	61.44	41.26	79.89	55.32	
Ethane (mole %)	0.34	0.15	1.69	1.26	2.66	1.66	
Propane (mole %)	0.69	0.29	0.23	0.25	0.47	0.37	
pH	6.90		6.70				7.10
Na (mg/L)	51230		53450				55150
K (mg/L)	3370		3450				3720
Ca (mg/L)	15290		15290				15430
Mg (mg/L)	2550		2160				2130
Sr (mg/L)	671		705				884
Cl (mg/L)	122707		123068				117743
HCO_3 (mg/L)	576		479				315
SO_4 (mg/L)	390		387				577
H_2S (aq) (mg/L)	560		660				177
TDS (mg/L)	197344		199649				196004

In June and September 2008, additional fluid and gas samples were collected from the source water well (100/11-29-045-02W5). The gas composition, water chemistry and isotopic composition of water, dissolved constituents and gases were determined at the University of Calgary and results are summarized in Table 4.

Table 4: Gas composition, water chemistry and isotopic composition of water, dissolved constituents and gases of samples obtained from well 100/11-29-045-02W5 in summer 2008.

Description	Value	Description	Value
pH	6.43	S^{2-} (mg/L)	171
Total Alkalinity (mg/L)	577	Total Dissolved Solids (mg/L)	197074
Na (mg/L)	55150	Electrical Conductivity (mS/cm)	129
Ca (mg/L)	15430	$\delta^{34}S$ in SO_4 (‰)	22.9
K (mg/L)	3720	$\delta^{34}S$ in S^{2-} (‰)	16.1
Mg (mg/L)	2129	$\delta^{13}C$ in HCO_3 (‰)	-8.2
Sr (mg/L)	884	CH_4 (mole %)	55.32
Mn (mg/L)	0.51	CO_2 (mole %)	5.00
Si (mg/L)	12.0	H_2S (mole %)	36.01
Cl (mg/L)	117743	$\delta^{13}C$ in CO_2 (‰)	-7.0
SO_4 (mg/L)	470	$\delta^{34}S$ in H_2S (‰)	16.1

1.2 Regional Baseline Geochemistry

The data summarized in Tables 1 and 2 were plotted and contoured over the WASP area (Figures 2–7). The black dots on the maps represent the locations of the wells for which data were available. The large red dot shows the location of the water source well (100/11-29-045-02W5). Data for fluids and gases from this well were not used for contouring.

1.2.1 Chemical Composition

Figure 2 shows the maps for total dissolved solids (TDS) and pH. The TDS map indicates high TDS values in the Nisku formation varying from less than 125,000 mg/L to more than 200,000 mg/L. There is a NE-SW gradient across the study area with high TDS values in the SW exceeding 200,000 mg/L and TDS values decreasing below 125,000 mg/L towards the NE. Fluids from the water source well had constant TDS values between 196,000 and 200,000 mg/L between 2003 and 2008 (Tables 3 and 4).
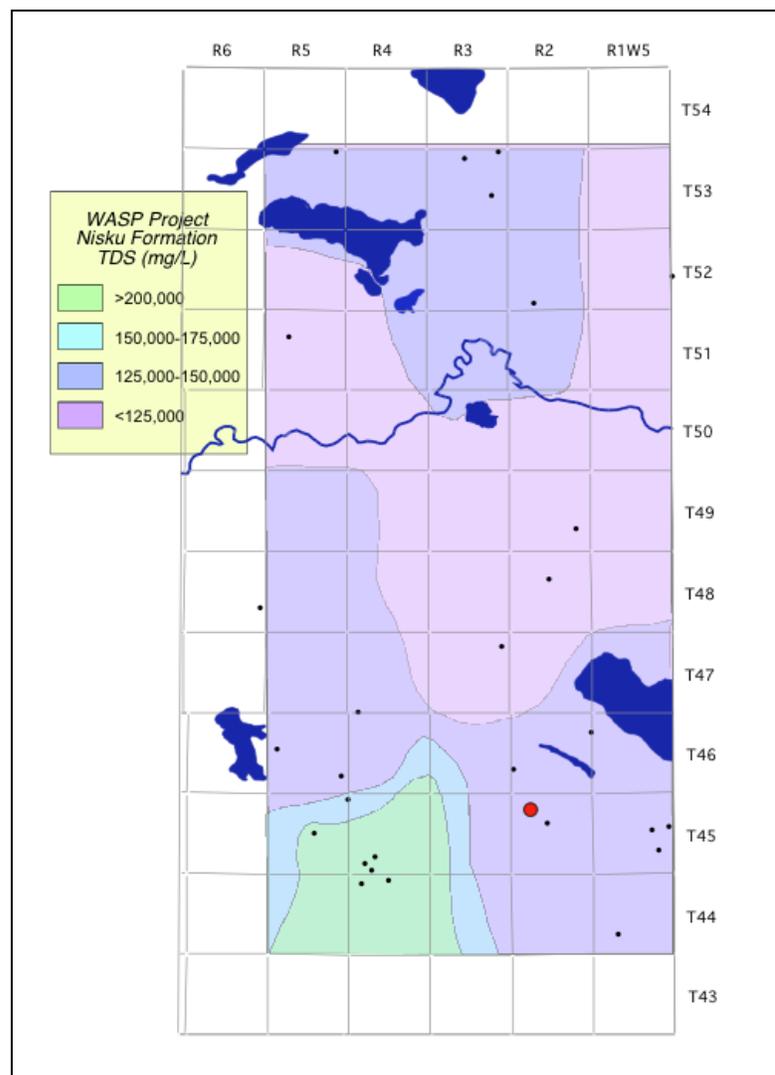
Figure 2a: WASP contour plots of total dissolved solids (TDS).
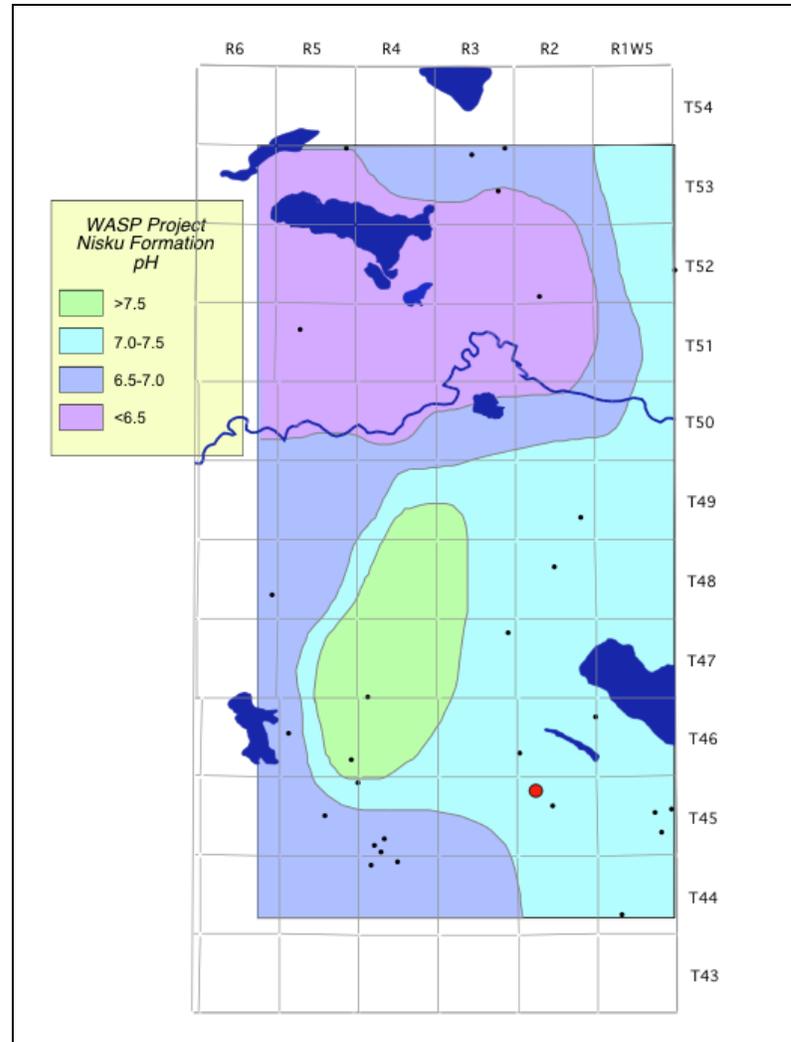
Figure 2b: WASP contour plots of pH values.

The pH map shows near neutral pH values across the study area (Figure 2) consistent with the measured pH value of 6.4 for fluids from the water source well (Table 4). The measured pH may be slightly biased towards higher values if samples were not preserved for dissolved sulphide, a very reactive species. When $H_2S_{(gas)}$ degasses from the sample the pH will increase towards a neutral value.

The fluid samples are Na-Cl brines and Figure 3 shows contour maps for sodium and chloride concentrations. Both of these maps show the same NE-SW concentration gradient as the TDS map. Na concentrations range from more than 55,000 mg/L in the SW to less than 50,000 mg/L in the central and northern part of the study area and Cl concentrations vary from more that 120,000 mg/L in the SW to less than 100,000 mg/L elsewhere. Fluids from the water source well had sodium concentrations between 51,000 and 55,000 mg/L and chloride concentrations between 118,000 and 123,000 mg/L (Table 3).
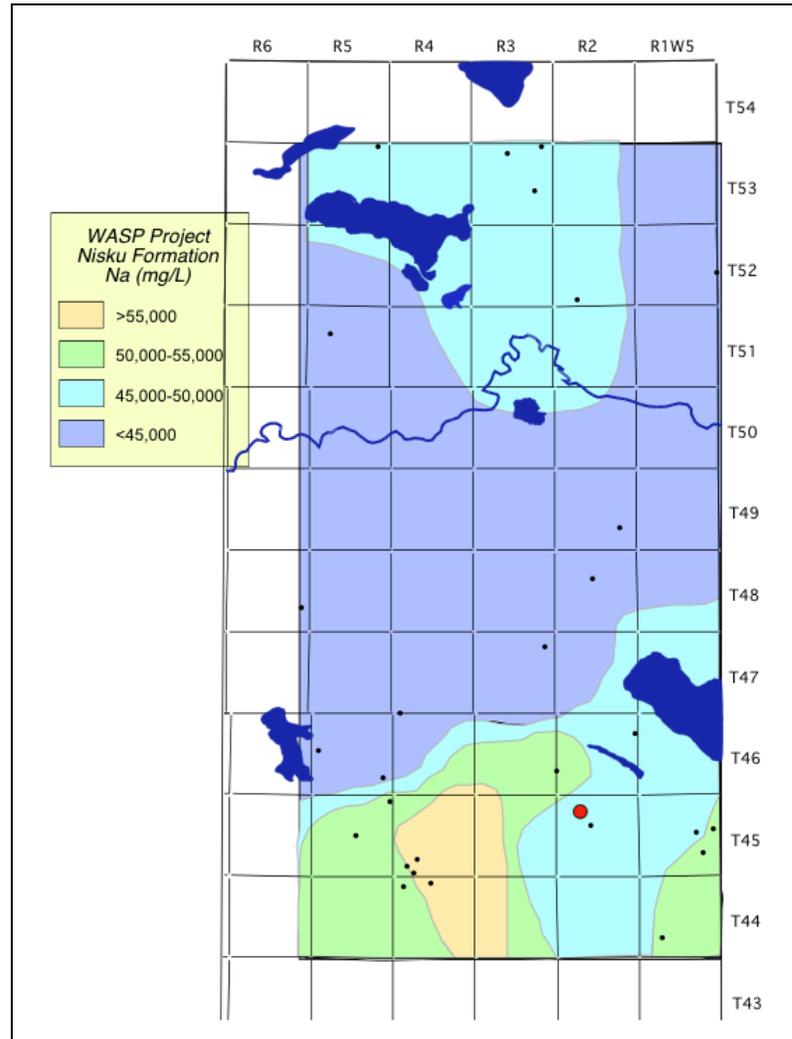
Figure 3a: WASP contour plots of sodium concentrations.
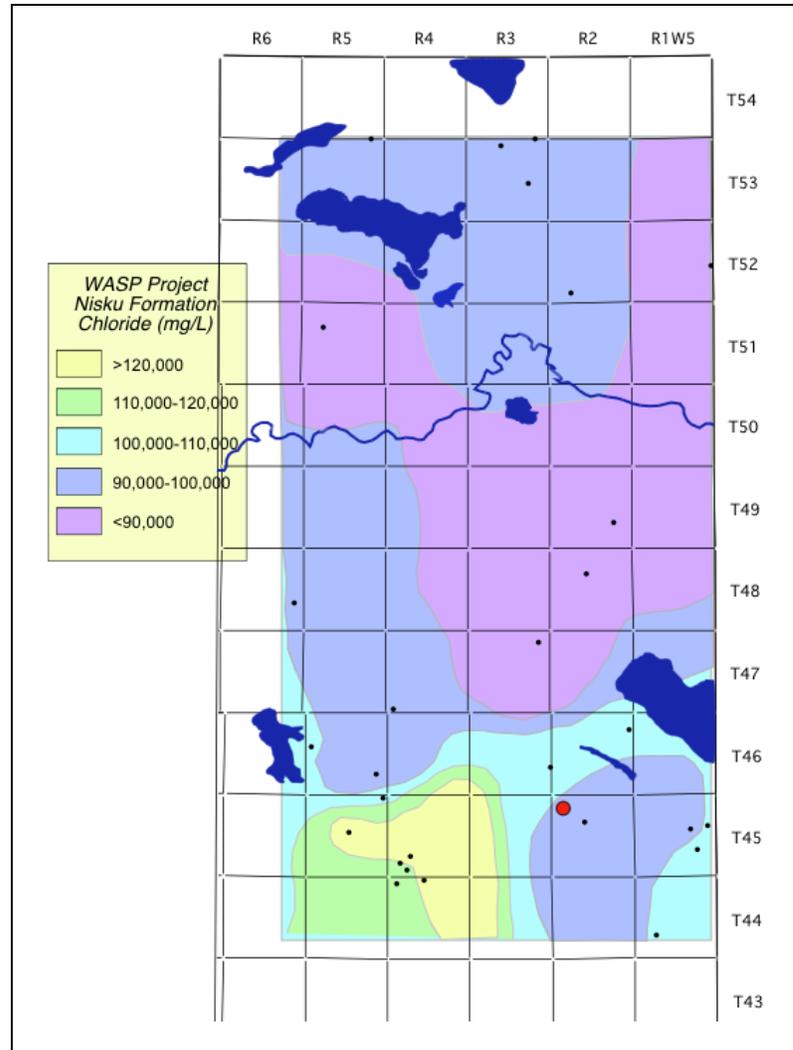
Figure 3b: WASP contour plots of chloride concentrations.

Figure 4 summarizes calcium and bicarbonate concentrations for the WASP study area. Ca concentrations vary from more than 15,000 mg/L in the SW to less than 12,500 in the central and northern part of the study area. Bicarbonate (HCO_3^-) concentrations are low throughout the study area not exceeding 1,000 mg/L. Fluids from the water source well have calcium and bicarbonate concentrations of 15,430 and 577 mg/L respectively.
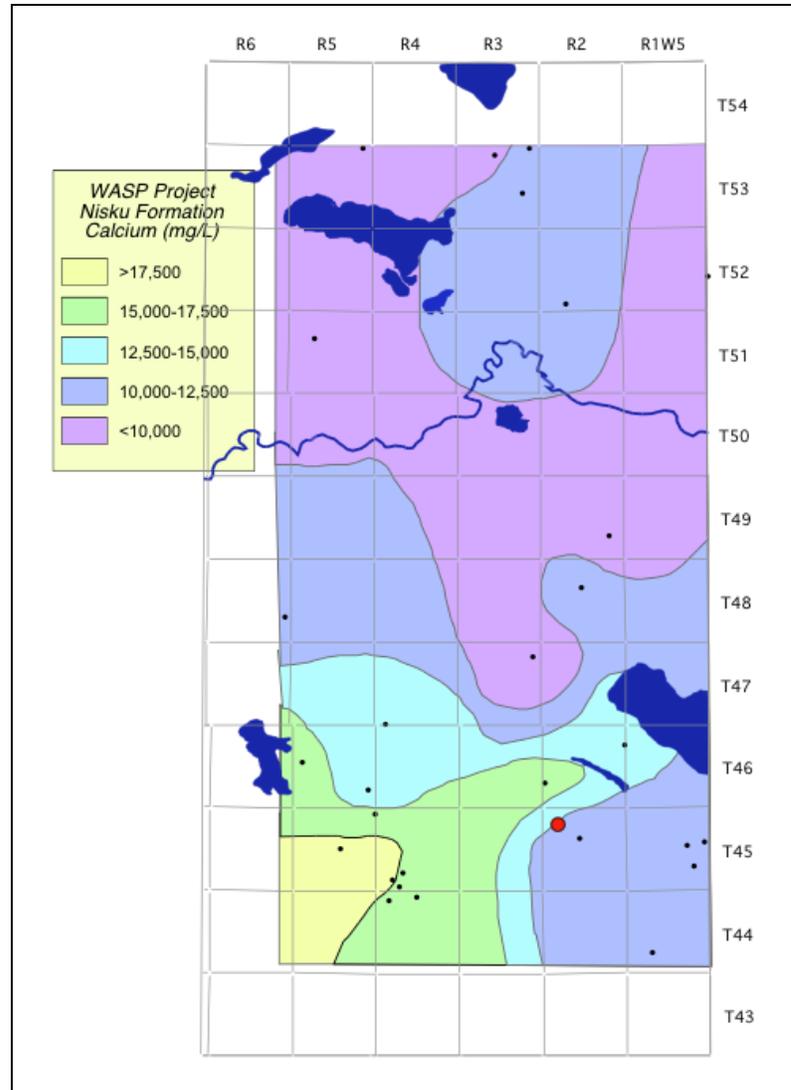
Figure 4a: WASP contour plots showing calcium concentrations.
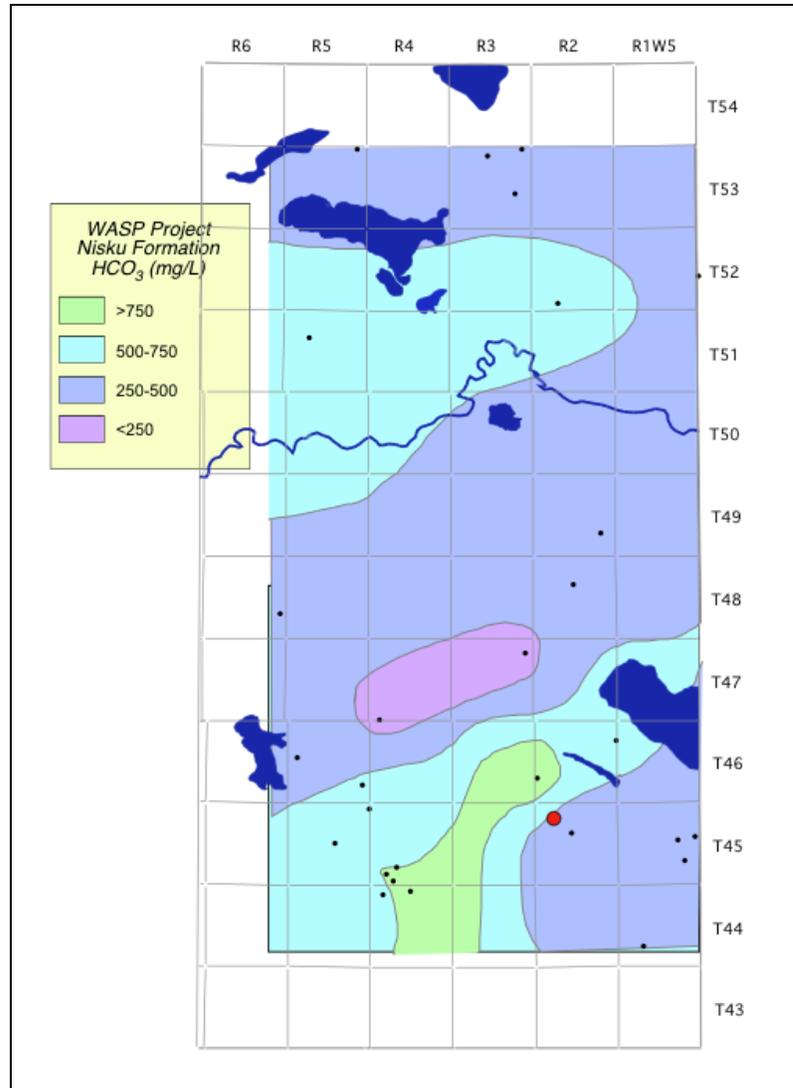
Figure 4b: WASP contour plots showing HCO_3 concentrations.

1.2.2 Isotopic Composition

Figure 5 shows contour maps of δ^{13}C-HCO$_3$ and δ^{34}S-SO$_4$ values using data obtained from Simpson's Ph.D. thesis *[5]*. The WASP study area is outlined in red on the map and the red dot represents the only location for which isotope data are available in the study area. The δ^{13}C-HCO$_3$ value determined for the sample from the water source well of -8.2 ‰ is within the range of carbon isotope ratios observed for dissolved inorganic carbon in the vicinity of the study area ranging from -10 to 0 ‰ (Figure 5). The δ^{34}S-SO$_4$ value of 22.9 measured for the sample from the water source well is also consistent with sulfur isotope ratios of < 25 ‰ in the vicinity of the southern part of the study area (Figure 5). Towards the northeast, there appears to be a trend of increasing δ^{34}S values for dissolved sulfate but the rate of change shown in Figure 5 is highly speculative due to lack of data in the northern portion of the WASP study area.
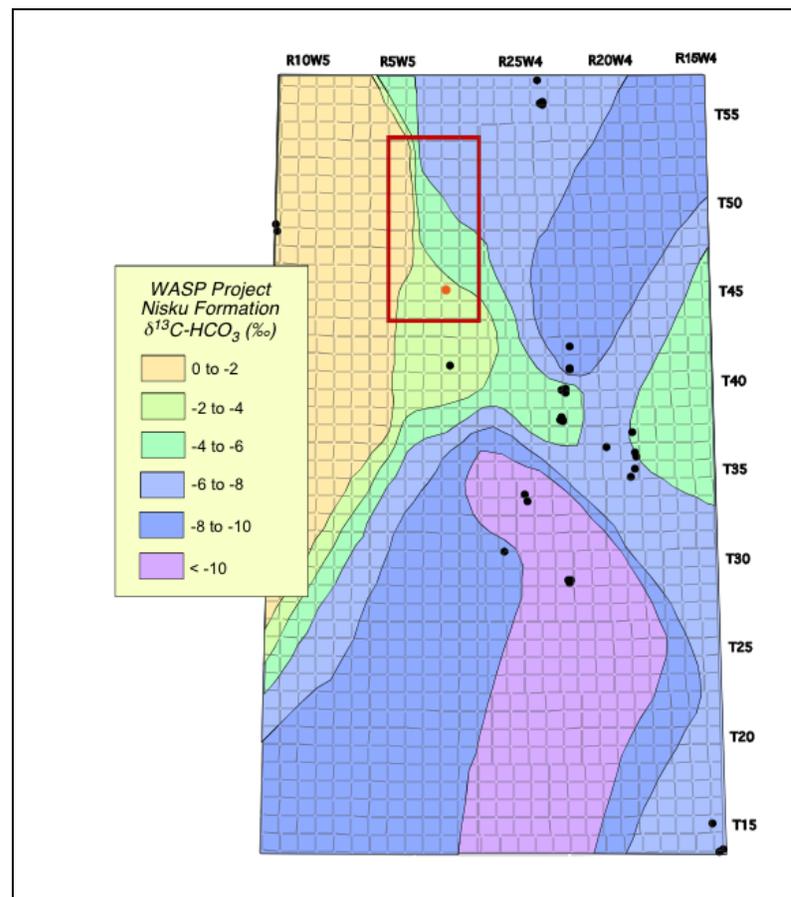
Figure 5a: Contour plots showing δ^{13}C-HCO$_3$ values for Nisku fluids sampled in the vicinity of the WASP study area.
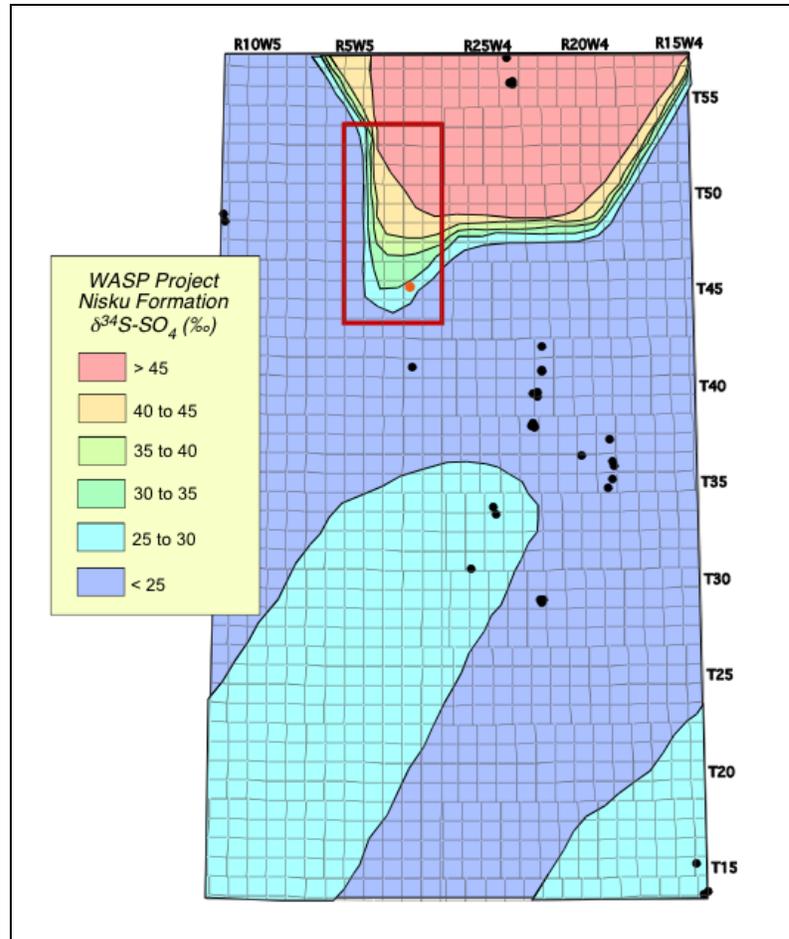
Figure 5b: Contour plots showing δ^{34}S-SO$_4$ values for Nisku fluids sampled in the vicinity of the WASP study area.

Figure 6 shows the contour plot for $\delta^{34}S$ values of dissolved sulphide (S^{2-}) from Simpson's data set *[5]*. The measured $\delta^{34}S$-S^{2-} value of 16.1 ‰ for the sample from the water source well in the study area is in excellent agreement with sulphur isotope values for dissolved sulphide in the vicinity of the WASP study area ranging from 15 to 20 ‰.

$\delta^{34}S$ values near +23 ‰ for dissolved sulphate are consistent with dissolution of Devonian anhydrite as the dominant sulphate source. The presence of significant quantities of H_2S with $\delta^{34}S$ values only 7 ‰ lower than those of dissolved sulphate indicates that thermo-chemical sulphate reduction (TSR) must have occurred *[5]*.
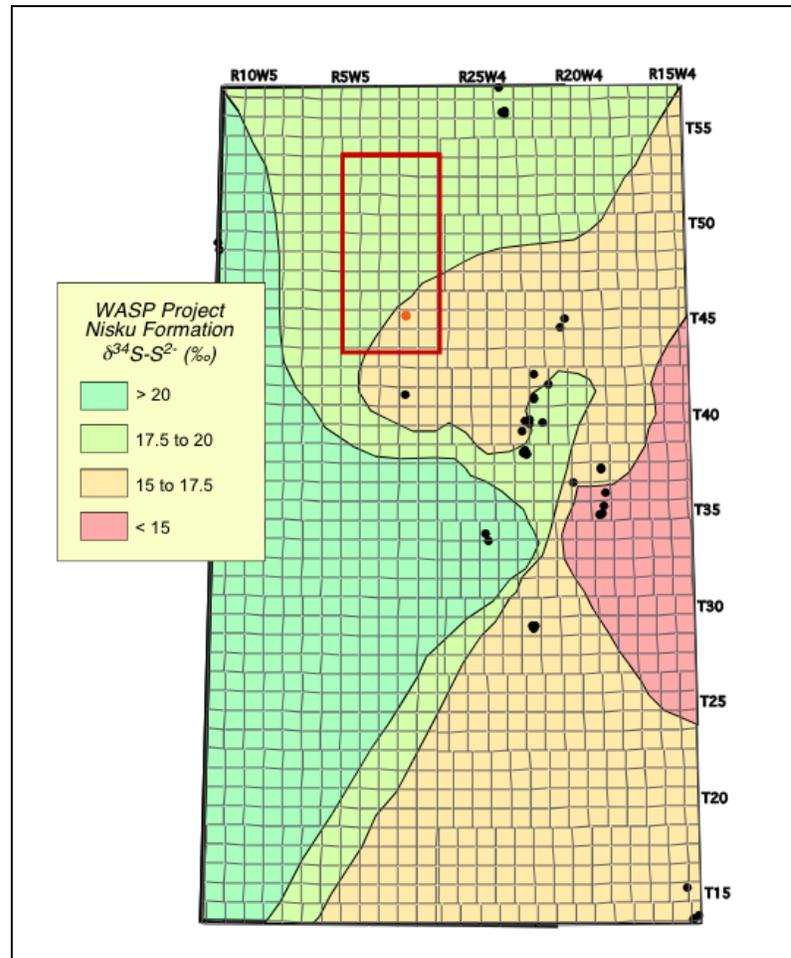
Figure 6: Contour plot of $\delta^{34}S$-S^{2-} values obtained from *[5]*.

1.3 Geochemistry of Fluids and Gases from the Water Source Well

Table 3 summarizes the data collected for fluids and gases obtained from well 100/11-29-045-02W5 during its initial completion in 2003 and 2004 as well as the data collected during two sampling trips in 2008. Figure 7 shows the evolution of the gas composition over this time period. Initially, the gas was predominantly composed of nitrogen (97 mole %) likely as an artifact of well construction and completion. Thereafter, methane (41-80 mole %) and H_2S (9-49 mole %) were the major constituents with CO_2 and N_2 representing less than 6 and 4 mole %, respectively. Gas production rates are not available for this well.

The results of chemical analyses conducted in 2008 are in excellent agreement with the historical data (Table 3). Total dissolved solids (TDS) remained constant around 196,000 mg/L, indicating that the concentration of the major dissolved species Na, Ca, K and Cl in the water had not changed significantly over the five-year observation period. The concentration of dissolved sulphide ($H_2S_{(aq)}$) collected at the well head varied between 177 and 660 mg/L (see section 3.2 for conversion to down-hole conditions). Sulphur isotope data suggest that H_2S is formed via thermo-chemical sulphate reduction (TSR) [5].
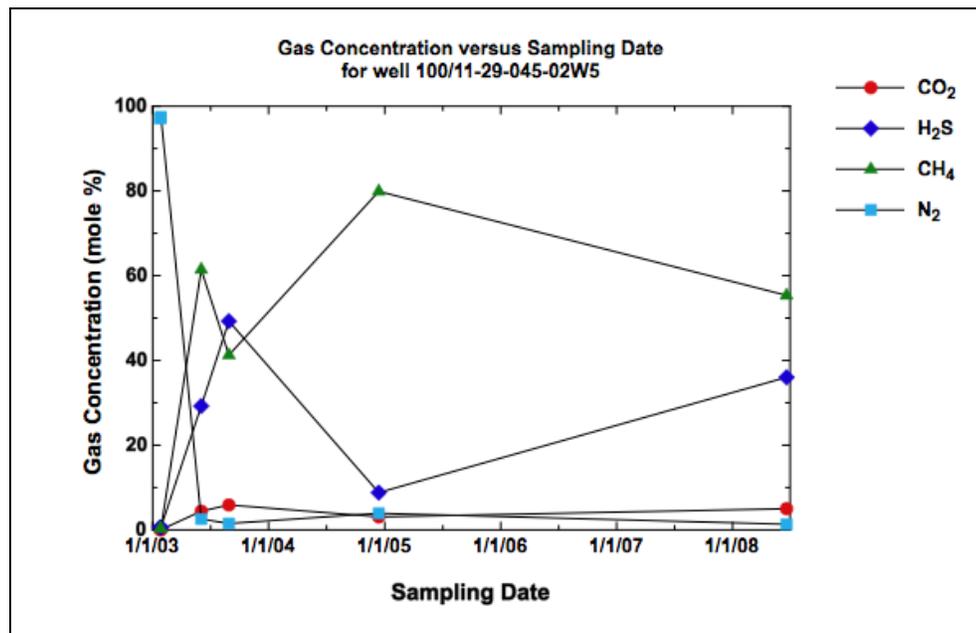
Figure 7: Gas concentration versus sampling date for four gases from well 100/11-29-045-02W5.

2.   MINERALOGY

To reach the goals of this project it was important to determine the mineralogical composition of the aquifer rocks and the caprock in the WASP study area.

2.1   Sample Selection and Methods

Twelve samples were collected from archived core from both the Nisku (eight samples) and Calmar (four samples) formations. The eight samples collected from the Nisku Formation included two separate lithofacies: i.e., four samples were collected from an open marine lithofacies, and four samples were collected from a hyper-saline lithofacies.

Samples collected were subdivided at the University of Calgary, i.e., approximately one third of the sample was archived, one-third was used for thin-section preparation, and one third was ground for whole rock geochemistry. Polished thin-sections for each of the twelve samples were prepared by Calgary Rock and Material Services (Calgary, Alberta). Thin-section analysis was completed at the University of Calgary using a Nikon Optiphot polarizing microscope, and a Jeol JXA-8200 electron microprobe in energy dispersion (EDS) mode. Bulk chemical analyses, including: X-ray Fluorescence (XRF), Inductively Coupled Plasma-Atomic Emission Spectrometry (ICP-AES), X-ray Diffraction (XRD), total carbonate, and total sulfur analysis, was completed by SGS Laboratories (Lakefield, Ontario).

Quantitative mineralogy was determined using linear programming normative analysis (LPNORM [7]) at the University of Calgary in consultation with Dr. John Bloch of the University of New Mexico, Albuquerque, New Mexico, USA. Carbon isotope ratios of carbonate rocks ($^{13}C/^{12}C$) were determined in the Isotope Science Laboratory at the University of Calgary using standard techniques.

2.2 Bulk Chemical Composition

The bulk chemical composition (major constituents) of each of the twelve samples analyzed is summarized in Table 5.

Table 5: Bulk Chemical Composition of Individual Core Samples (Ni = Nisku, C = Calmar).

Sample	Formation	SiO_2%	Al_2O_3%	Fe_2O_3%	MgO%	CaO%	K_2O%	CO_2%	S%
W1	Ni	3.1	0.6	0.3	20.2	30.6	0.2	45.3	0.0
W2	Ni	1.9	0.8	0.3	18.5	32.8	0.3	44.8	0.0
W3	Ni	35.0	2.7	2.2	12.4	18.2	1.4	26.9	0.7
W4	Ni	1.4	0.2	0.2	10.8	36.0	0.1	23.6	11.0
W5	Ni	2.1	0.2	0.3	18.7	32.0	0.1	45.1	0.1
W6	Ni	0.6	0.1	0.1	21.4	30.9	0.1	45.9	0.2
W7	Ni	1.1	0.2	0.5	20.8	30.3	0.1	45.3	0.1
W8	Ni	0.5	0.2	0.2	21.0	30.5	0.1	45.8	0.0
W9	C	70.5	12.0	2.9	2.3	1.1	5.1	1.5	0.9
W10	C	70.3	9.8	2.2	2.8	2.5	4.6	3.6	0.8
W11	C	68.8	13.5	3.5	1.8	0.3	5.8	0.2	1.4
W12	C	72.9	11.8	2.8	1.7	0.4	5.1	0.2	1.0

The results are consistent with the known lithologies of the two formations, i.e., samples from the Calmar Formation (9-12) are shale/mudstones and composed primarily of aluminium and silicon oxides; samples from the Nisku Formation (1-8) are predominantly dolomite and composed primarily of calcium, magnesium and carbonate. Two exceptions within the Nisku group include: Sample 3, which contained a significant amount of silicon, aluminum, and potassium; and Sample 4, which contained a significant amount of sulfur and calcium relative to the rest of the group suggesting the presence of anhydrite. There were no discernable differences between the two separate lithofacies (open marine and hyper-saline) of the Nisku Formation.

The carbon isotope ratios of carbonate ($\delta^{13}C$) of the eight samples from the Nisku Formation were determined and results are summarized in Table 6. The $\delta^{13}C$ values of the Nisku samples ranged from -4.4 to -6.9 ‰ and are lower than those of Late Devonian seawater (+2.0 to +3.0 ‰; [8]).

Table 6: Carbon isotope ratios of Nisku carbonates.

Sample	$\delta^{13}C_{carbonate}$ (‰)
W1	-4.4
W2	-4.9
W3	-6.9
W4	-4.6
W5	-4.5
W6	-5.3
W7	-5.6
W8	-4.7

The obtained $\delta^{13}C$ values for samples from the hyper-saline facies (samples 3, 4, 5 and 7) are consistent with those of Whittaker et al. *[9]*. These authors suggested that shelf carbonates reflect a more restricted environment than open marine, and that carbon isotope ratios of carbonate may be lower than those of open marine carbonates due to carbon input via organic matter respiration. It is

possible that the lower than expected $\delta^{13}C$ values for the open marine samples (samples 1, 2, 6 and 8) are in part the result of re-crystallization of the original deposit in the presence of ^{13}C depleted meteoric water *[9]*.

2.3 Microscopy

The presence and composition of major mineral phases was established by analysis of thin-sections using a conventional petrographic microscope and by electron microprobe.

The shales of the Calmar Formation consist of small clasts of quartz, feldspars (k-spar and albite), and micas (predominately muscovite) in a fine clay (illite) matrix (Figure 8). Finely disseminated pyrite was found in all four shale samples analyzed.
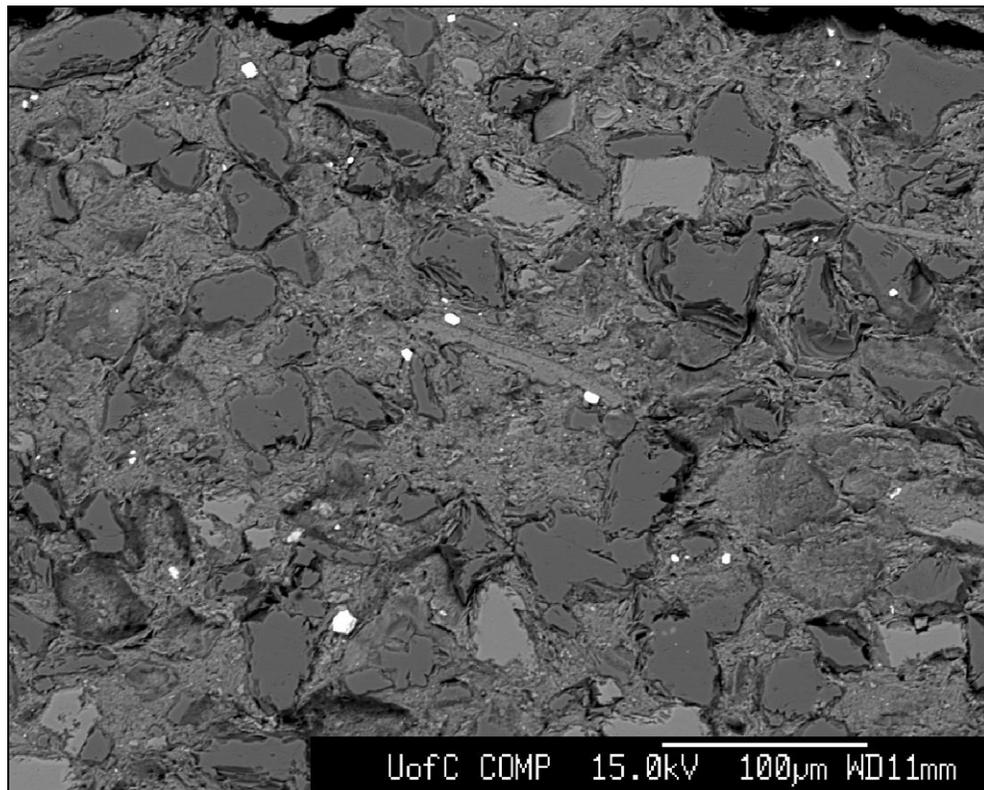
Figure 8: Photomicrograph of the Calmar Formation.

A photomicrogarph of a typical Nisku carbonate is shown in Figure 9. A significant amount of replacement dolomitization of the original limestone is evident in the eight samples of Nisku core analyzed.
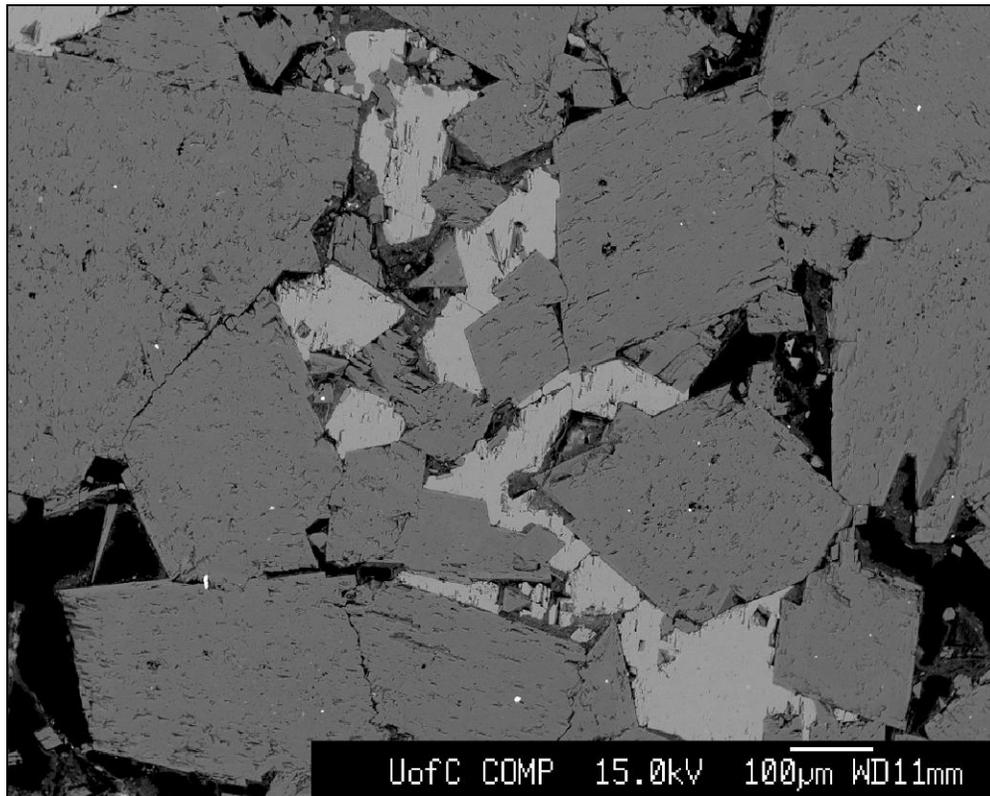
Figure 9: Photomicrograph of the Nisku Formation (Sample W12).

The residual limestone is composed of stoichiometric calcite i.e., composed largely of calcium and carbonate with very little substitution of magnesium, iron, manganese or strontium for calcium (Table 7).

Table 7: Average Composition of Nisku Formation Calcite (wt%).

CaO	MgO	FeO	MnO	SrO	CO_2
53.8	0.5	0.3	0.3	0.2	45.0

The replacement dolomite crystals are often compositionally zoned (Figure 10) with the outer crystal being slightly more calcium-rich relative to the inner crystal.
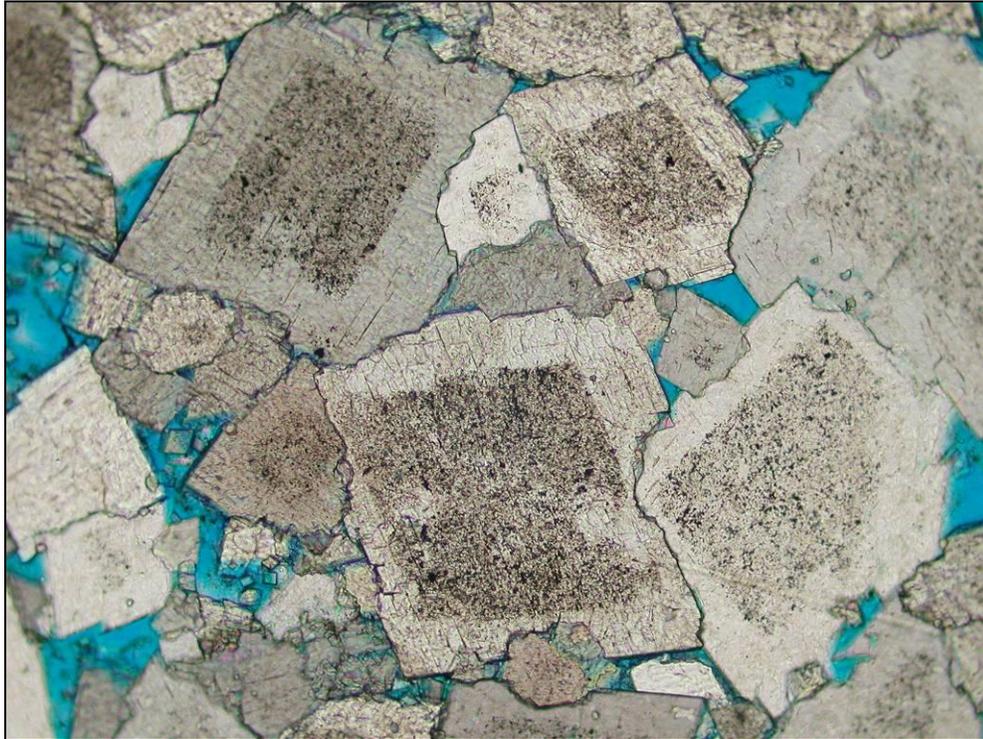
Figure 10: Photomicrograph of Zoned Dolomites (Sample W2).

The average composition of the Nisku Formation dolomite is presented in Table 8.

Table 8: Average Composition of Nisku Formation Dolomite (wt%).

CaO	MgO	FeO	MnO	SrO	CO_2
34.9	16.9	0.3	0.1	0.1	47.7

In samples composed primarily of carbonate rock, there were no discernable differences in either appearance or chemical composition between the two separate lithofacies (open marine and hyper-saline) of the Nisku Formation (Figures 11 and 12).
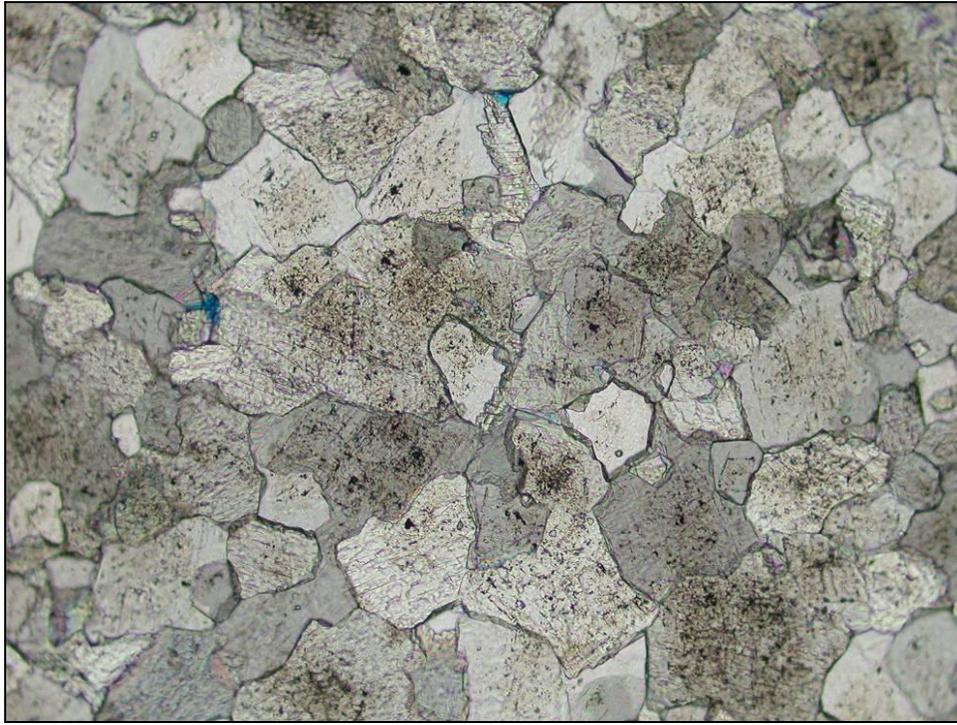
Figure 11: Photomicrograph of Nisku Open Marine Facies (Sample W6).
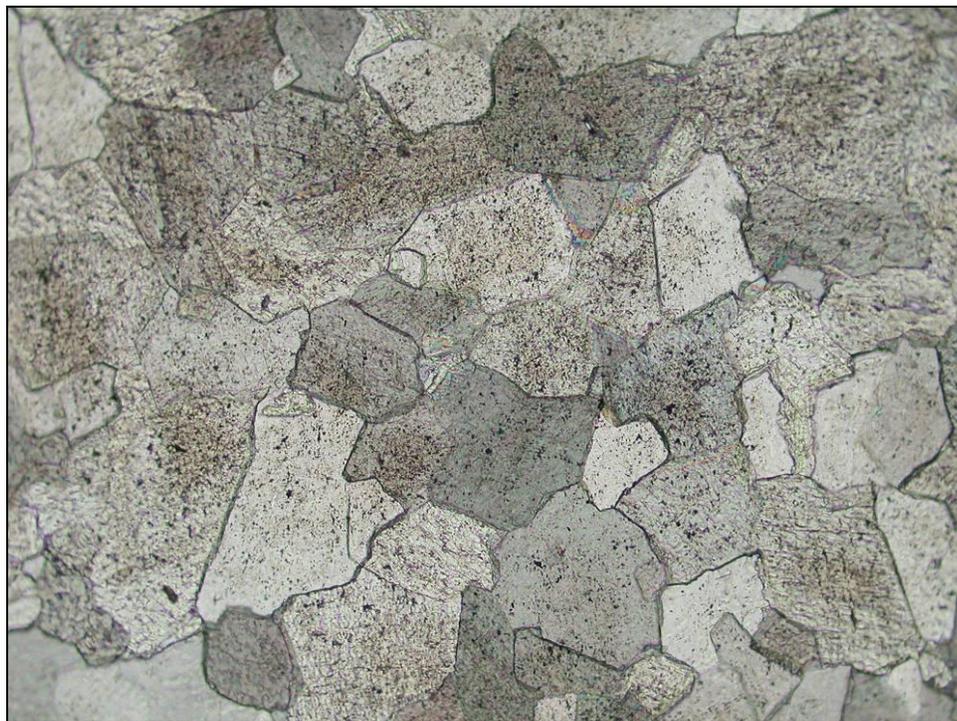
Figure 12: Photomicrograph of Nisku Hyper-Saline Facies (Sample W7).

Sample W3 (Figure 13) was found to contain a significant amount of detrital quartz, feldspar and mica (predominantly muscovite) in addition to dolomite.
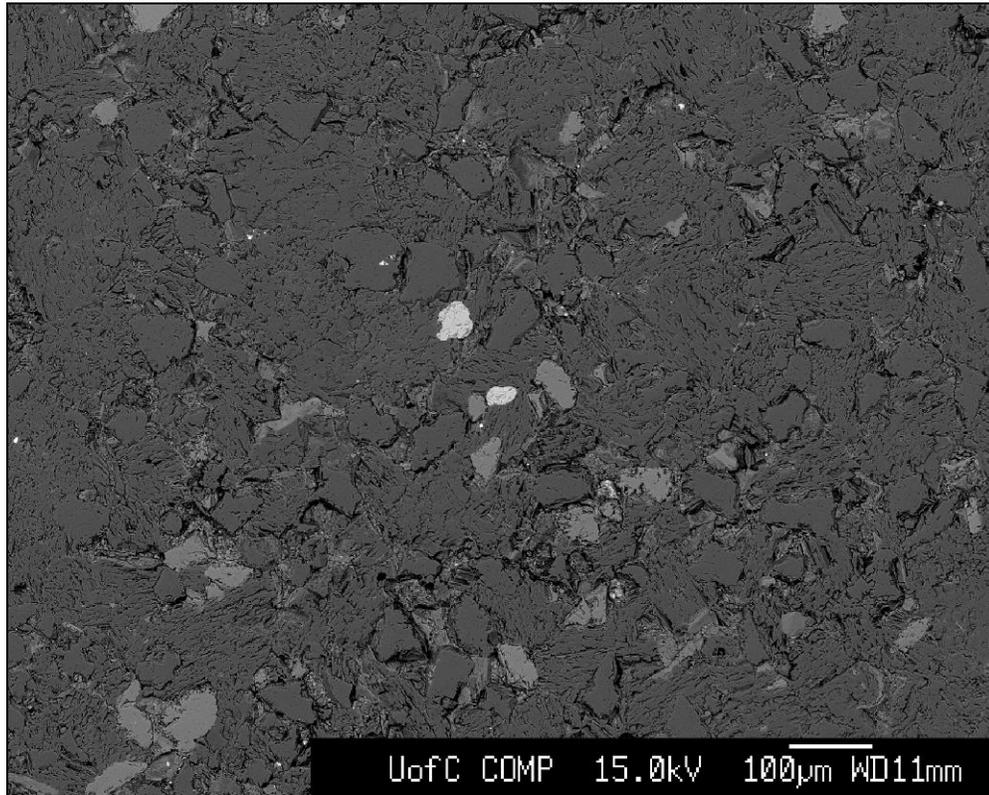
Figure 13: Photomicrograph of Nisku Sample W3.

A significant amount of anhydrite was observed in Sample W4 (Figure 14). The presence of anhydrite in the hyper-saline facies of the Nisku Formation was not unexpected. Machel *[10]* suggested that anhydrite is genetically related to the replacive dolomites present.
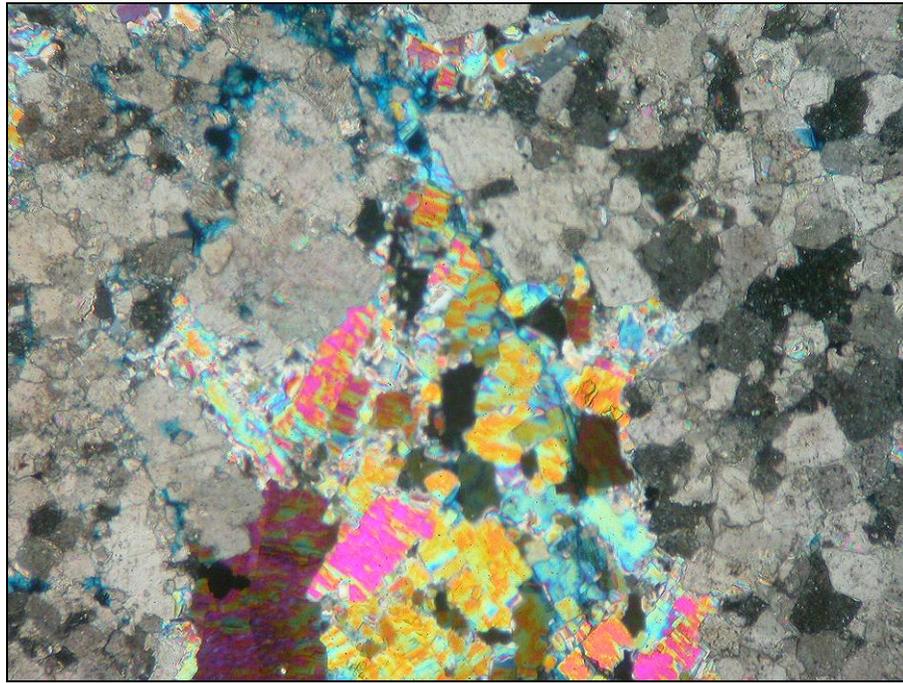
Figure 14: Photomicrograph of Nisku Anhydrite (Sample W4).

2.4 Quantitative Mineralogy

Quantitative mineralogy was determined using a linear programming normative analysis (LPNORM) program *[7]*. There are advantages to using LPNORM analysis over mineral point counting from thin sections, and/or XRD alone, i.e., LPNORM incorporates mineralogical information from several sources (polished thin-section examination, XRD, and electron microprobe) with whole-rock analysis (XRF, ICP, total carbonate, and total sulfur). The quantitative mineralogy of each of the twelve samples analyzed is summarized in Table 9.

Table 9: Quantitative Mineral Composition (wt%).

Sample	Calcite	Dolomite	Quartz	Albite	K-spar	Ill/Mus	Anhydrite	Pyrite
W1	6.2	89.2	2.0	0.0	0.2	2.0	0.0	0.0
W2	15.2	79.9	0.0	0.6	0.9	1.9	0.0	0.0
W3	3.8	52.9	27.6	1.7	5.1	4.4	0.0	1.3
W4	5.5	44.4	0.9	0.0	0.4	0.5	47.1	0.0
W5	11.7	83.8	1.4	0.5	0.6	0.0	0.0	0.2
W6	5.9	90.7	0.3	0.0	0.6	0.0	0.0	0.0
W7	5.1	90.2	0.4	0.5	0.3	0.0	0.0	0.2
W8	4.7	91.6	0.0	0.0	0.4	0.5	0.0	0.0
W9	0.5	2.7	43.4	2.5	14.9	29.6	0.0	1.7
W10	0.7	6.9	46.7	2.5	16.2	22.1	0.0	1.5
W11	0.0	0.4	37.8	3.4	17.6	33.5	0.1	2.6
W12	0.5	0.0	45.5	3.4	15.8	28.7	0.0	1.9

The average composition of the four Calmar Formation shales analyzed is: 43.4% quartz, 28.5% illite/muscovite, 16.1% k-spar, 3.0% albite, 2.5% dolomite, and 1.9% pyrite.

With the exception of samples 3 and 4, the Nisku samples are predominantly composed of dolomite (up to 91.6%), with smaller amounts of calcite (up to 15.2%) present. Sample 3, was found to contain 27.6% detrital quartz, and smaller amounts of detrital feldspars (6.8%), micas (4.4%), as well as dolomite (52.9%). Sample 4, contains a substantial amount of anhydrite (47.1%) as well as dolomite (44.4%).

Knowledge of the mineralogical composition of aquifer rocks and caprocks is an essential input parameter for geochemical modelling of the fate of injected CO_2 in the WASP study area.

3. GEOCHEMICAL MODELLING

3.1 SOLMINEQ88

Geochemical modelling was conducted using the sampled well water analysis summarized in Table 4 and the geochemical computer program SOLMINEQ88 *[11]* to determine the saturation indices of selected minerals. The saturation index (SI) measures the saturation state of a mineral phase whose chemical components are dissolved in the produced fluid. A mineral that yields SI < -0.3 is considered under-saturated and hence has the potential to dissolve. Conversely, a mineral that yields SI > 0.3 is considered over-saturated suggesting that the mineral may precipitate from the fluid. A SI value in the range of -0.3 < SI < 0.3 is generally accepted as being in equilibrium with the fluid. This range is somewhat arbitrary but is based on typical analytical accuracies and sample

variabilities, as well as the slower reaction rates of phases as they approach equilibrium. Actual mineral dissolution or precipitation is controlled by temperature-dependant kinetic reaction rates and by the reactive surface area of the mineral. The saturation index is an indication of the potential to dissolve or precipitate a mineral and does not necessarily mean that the predicted reaction is actually taking place at a significant rate.

The Nisku Formation is composed of dolostones (dolomite) and limestone (calcite). The Calmar caprock is predominantly composed of shales. The bottom rock is the Ireton, which is composed of calcareous shales and argillaceous limestone *[12]*.

Based on the chemical data summarized in Table 4, saturation indices for calcite, dolomite, anhydrite and quartz were determined and are summarized in Table 10 for the downhole pressure (17.5 MPa) and temperature (82.5 ºC) of the well. The SI for quartz fell within the equilibrium range, -0.3 < SI < 0.3, which is expected for an unperturbed reservoir. Anhydrite had a SI of -0.51 indicating that anhydrite has the potential to slowly dissolve. The two carbonate minerals, calcite and dolomite, have a positive SI, indicating the potential for carbonate mineral precipitation. Since CO_2 injection will result in increasing bicarbonate contents in the reservoir fluids, the potential for calcite and dolomite to precipitate will likely persist or increase.

Table 10: Saturation Indices for common minerals found in the Nisku formation, the Calmar caprock and the Ireton bottom-rock.

Mineral	Saturation Index
Calcite	0.45
Dolomite	1.09
Anhydrite	-0.51
Quartz	-0.10

3.2 H_2S Saturation Modelling

The measured concentrations of $H_2S_{(aq)}$ in produced waters collected at the well head are not identical to the H_2S content at reservoir conditions since H_2S exsolves during pumping of produced fluids to the well head. Therefore the actual down-hole H_2S content was determined using geochemical models. The solution obtained from the water source well was a 2.55 M NaCl solution. According to Duan et al. *[13]*, for a solution with a partial pressure of 16 MPa, 60ºC and 2.55 M NaCl, the solubility of H_2S in water is 1.63 moles per kg of water or 63,180 mg/L. When this water is moved from depth to the surface and depressurized to 101 kPa and 25ºC, the concentration of $H_2S_{(aq)}$ in the water decreases to 0.0678 moles per kg or 2,640 mg/L. Measured H_2S concentrations at the well head varied between 177 and 660 mg/L (Table 3). Based on a gas/water ratio of 4:1 (personal communication), and using the equations from Duan et al. *[13]*, the concentration of $H_2S_{(aq)}$ in the reservoir at depth and pressure at the time of sampling was calculated to be 0.069 moles per kg or 2,350 mg/L, which is significantly less than the saturation value of 63,180 mg/L. Thus the Nisku waters are under saturated with respect to $H_2S_{(aq)}$.

3.3 ToughReact Modelling

ToughReact *[14]* is a reactive transport code that uses chemically speciation and water-rock-gas interaction calculations as well as multidimensional non-isothermal multiphase flow and mass transport. It is used to simulate deep saline aquifer storage of CO_2 *[15]*. Here, this code has been used to simulate the geochemical processes occurring in two reservoirs where CO_2 injection is occurring, one with H_2S present and the other without.

3.3.1 Problem Setup

A single layer uniform carbonate formation with a thickness of 70 m is considered in the present model. The hydrological parameters of the formation are representative of those for a carbonate formation. The formation is assumed to be uniform throughout and extends infinitely in the horizontal direction. A non-uniform radial grid is used with spacing increasing away from the well.

This fluid flow is a very simple model, i.e., a first order model, and does not consider formation heterogeneities that would result in non-uniform sweeps or buoyancy forces that would tend to drive the CO_2 towards the top of the aquifer. Initially, injected CO_2 will tend to accumulate and spread out near the top of the permeable layer and will partially dissolve in the aqueous layer. The dissolution of the CO_2 in the aqueous layer will cause its density to increase over time and will eventually give rise to buoyancy driven convection where CO_2 enriched waters will migrate downward *[16]*. The dissolution process and aqueous phase convection will vertically mix the aqueous CO_2 with a mixing time scale on the order of hundreds of years or more *[17]* and is similar to the time scales for significant interactions of CO_2.

The hydrogeological parameters used in the simulations are summarized in Table 11. The carbonate formation was assumed to be homogeneous. Injection of carbon dioxide was simulated at 31.69 kg/s (1 MT/year) for 50 years. The initial pressure was 16 MPa at the top of the formation. In all simulations the initial reservoir pressure was set at 17.5 MPa, formation temperature of 60ºC, a permeability of 30 mD and a porosity of 10%. The simulations were conducted over a 50-year injection period where the injection rate was 1MT/year of CO_2 or 31.69 kg/sec.

The initial mineral composition used in the modelling is consistent with samples from well 2 (see section 2) as summarized in Table 12. The kinetic data for orthoclase were not available and therefore a substitution of k-feldspar was made. Since H_2S is present in the reservoir, secondary minerals, such as pyrite, were chosen. Also chosen as a secondary mineral was magnesite given that significant amounts of magnesium may be released from dolomite dissolution.

The water composition used is that measured for fluids from the water source well summarized in Table 4. The water composition given in Table 4 is representative for surface conditions, i.e., after the sample degassed while moving from depth to surface. The water used in the simulation was re-equilibrated with the degassing H_2S, CH_4 and CO_2 using SOLMINEQ88 *[11]* as shown in Table 12. Two species shown in Table 13 were not measured, AlO_2^- and $O_{2(aq)}$. A small amount of each was added since the first would probably be present due to the presence of silicate minerals and $O_{2(aq)}$ was necessary for redox reactions to occur.

Table 11: Hydrogeological parameters for the Nisku carbonate formation.

Parameter	
Permeability (m^2)	0.3×0^{-13}
Porosity	0.10
Temperature (ºC)	60
Pore Compressibility (Pa^{-1})	$4.5\ 10^{-10}$
Tortuosity [21]	0.3
Compressibility (Pa^{-1}) [21]	$1\ 10^{-8}$
Diffusivity (m^2/s) [21]	$1\ 10^{-9}$
Relative Permeability	
Liquid [18] $k_{rl} = \sqrt{S^*\{1-(1-[S^*]^{1/m})^m\}^2}$ S_{lr} : irreducible water saturation m: exponent	$S^* = (S_l - S_{lr})/(1 - S_{lr})$ $S_{lr} = 0.3$ m=0.457
Gas [19] $k_{rg} = (1-\hat{S})^2(1-\hat{S}^2)$ S_{gr} : irreducible gas saturation	$\hat{S} = (S_l - S_{lr})/(S_l - S_{lr} - S_{gr})$ $S_{gr} = 0.05$
Capillary Pressure	
[18] $P_{cap} = -P_0([S^*]^{-1/m} - 1)^{1-m}$ S_{gr} : irreducible gas saturation m: exponent P_0 : strength coefficient (kPa)	 $S_{lr} = 0.0$ m=0.457 $P_0 = 19.61$

Table 12: Initial mineral volume fractions and possible secondary minerals used in the ToughReact simulations.

Mineral	Chemical Formula	Volume % of Solid	Volume % of Medium
Primary			
Dolomite	$CaMg(CO_3)_2$	81.22	80.49
Calcite	$CaCO_3$	15.45	16.04
Illite	$K_{0.6}Al_{1.8}Mg_{0.25}(Al_{0.5}Si_{3.5}O_{10})(OH)_2$	1.89	1.89
K-feldspar	$KAlSi_3O_8$	0.86	0.95
Low-Albite	$NaAlSi_3O_8$	0.58	0.62
Secondary			
Kaolinite	$Al_2Si_2O_5(OH)_4$		
Na-smectite	$Na_{0.29}Mg_{0.26}Al_{1.77}Si_{3.97}O_{10}(OH)_8$		
Ca-smectite	$Ca_{0.145}Mg_{0.26}Al_{1.77}Si_{3.97}O_{10}(OH)_8$		
Dawsonite	$NaAlCO_3(OH)_2$		
Aragonite	$SrCO_3$		
Siderite	$FeCO_3$		
Ankerite	$CaMg_{0.3}Fe_{0.7}(CO_3)_2$		
Magnesite	$MgCO_3$		
Pyrite	FeS_2		

Table 13: Initial total dissolved chemical species concentrations used in the ToughReact simulations.

Species	Concentration (mol/kg)
pH	6.10
Ca^{2+}	0.41
Mg^{2+}	9.33×10^{-2}
Na^+	2.56
K^+	0.10
Sr^{2+}	1.08×10^{-2}
Fe^{2+}	9.35×10^{-6}
$SiO_{2(aq)}$	4.56×10^{-4}
HCO_3^-	2.01×10^{-2}
SO_4^{2-}	5.21×10^{-3}
Cl^-	3.44
AlO_2^-	1.36×10^{-7}
$O_{2(aq)}$	4.88×10^{-70}
$H_2S_{(aq)}$	3.97×10^{-2}

Two groups of simulations were preformed. The first group was for an aquifer with the mineralogical composition listed in Table 12 and the water composition listed in Table 13 with no $H_2S_{(aq)}$ present. The second group was identical but included $H_2S_{(aq)}$.

Table 14 provides the parameters for the kinetics of dissolution and precipitation for the minerals used in the models [20]. Calcite was used as an equilibrium mineral in the simulations. Specific details about the kinetics used in the simulations can be found in Xu et al. [21].

Table 14: Parameters for calculating kinetic rate constants of minerals used in the simulations [20].

Mineral	A (cm²/g)	Neutral Mechanism		Acid Mechanism			Base Mechanism		
		k^{25} (mol/m²/s)	E (kJ/mol)	k^{25}	E	$n(H^+)$	k^{25}	E	$n(H^+)$
Dolomite	9.1	$2.9512\ 10^{-8}$	52.2	$6.4565\ 10^{-04}$	36.1	0.500			
Illite	108.7	$1.6596\ 10^{-13}$	35.0	$1.0471\ 10^{-11}$	23.6	0.340	$3.02\ 10^{-17}$	58.9	-0.400
K-feldspar	9.1	$3.8905\ 10^{-13}$	38.0	$8.7096\ 10^{-11}$	51.7	0.500	$6.3096\ 10^{-22}$	94.1	-0.823
Low-Albite	9.1	$2.7542\ 10^{-13}$	69.8	$6.9183\ 10^{-11}$	65.0	0.457	$2.5119\ 10^{-16}$	71.0	-0.572
Kaolinite	108.7	$6.9183\ 10^{-14}$	22.2	$4.8978\ 10^{-12}$	65.9	0.777	$8.9125\ 10^{-18}$	17.9	-0.472
Nasmectite	108.7	$1.6596\ 10^{-13}$	35.0	$1.0471\ 10^{-11}$	23.6	0.340	$3.0200\ 10^{-17}$	58.9	-0.400
Casmectite	108.7	$1.6596\ 10^{-13}$	35.0	$1.0471\ 10^{-11}$	23.6	0.340	$3.0200\ 10^{-17}$	58.9	-0.400
Dawsonite	9.1	$1.2598\ 10^{-09}$	62.76	$6.4565\ 10^{-04}$	36.1	0.500			
Aragonite	9.1	$4.5709\ 10^{-10}$	23.5	$4.1687\ 10^{-07}$	14.4	1.000			
Siderite	9.1	$1.2598\ 10^{-09}$	62.76	$6.4565\ 10^{-04}$	36.1	0.500			
Ankerite	9.1	$1.2598\ 10^{-09}$	62.76	$6.4565\ 10^{-04}$	36.1	0.500			
Magnesite	9.1	$4.5709\ 10^{-10}$	23.5	$4.1687\ 10^{-07}$	14.4	1.000			
Pyrite	12.87	$2.8184\ 10^{-05}$	56.9 $n(O_{2(aq)}) = 0.5$	$3.2022\ 10^{-08}$	56.9 $n(H^+) = -0.5$, $n(Fe^{3+}) = 0.5$				

Notes: (1) all rate constants are for dissolution

(2) A is specific area, k^{25} is kinetic rate constant at 25ºC, E is activation energy, n is power term (Eq. (3), [21])

(3) power terms n for both acid and base mechanism are with respect to H^+

(4) for pyrite, the neutral mechanism has n with respect to O2(aq), the acid mechanism has two species involved: one n with respect to H+ and another n with respect to Fe3+ (Eq. (3), [21])

3.3.2 Results

The output from the ToughReact simulations consists of information in three categories:

1. compositions of the aqueous phase,
2. distribution of primary and secondary minerals,
3. physical properties of the system, e.g., porosity.

Data presented in this report is for four time periods, 1 year, 10 years, 25 years and 50 years of injection over a radial distance of up to 10,000 metres.

The pH distribution along the radial distance is shown in Figure 15. For all the simulations the pH increases from a low value to 5.1 at a distance of 19.7 m after year 1, remains constant for a distance of ~500 m, and increases again to ~6.4 while remaining constant over the rest of the radial distance. This pattern was observed for both H_2S and non-H_2S aquifers. With increasing time after CO_2 injection, the distance of the initial pH increase changed from 19.7 m after year 1 to 146 m after 50 years. The second increase of pH values changed from an initial distance of ~500 m for year 1 to ~5000 m after 50 years.
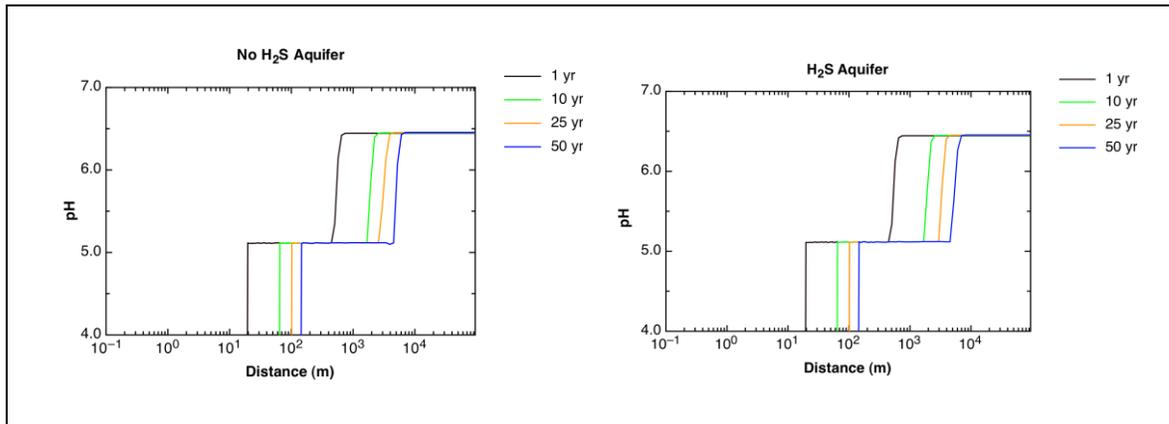
Figure 15: pH of aquifer as a function of radial distance after initiation of CO_2 injection for both non-H_2S and H_2S aquifers.

Figure 16 shows the concentration of bicarbonate (in moles/kg) as a function of distance. The initial concentration of bicarbonate in the water is 0.02 moles/kg across the entire modelling area. After one year, the concentration of bicarbonate in the water increased to ~1.25 moles/kg at a distance of 19.7 m from the injector and remained elevated to a distance of ~500 m. Thereafter bicarbonate concentrations decreased to baseline values (~0.02 moles/kg). A similar pattern of increasing and decreasing bicarbonate concentrations was observed after 10, 25 and 50 years at increasing distances from the injector.
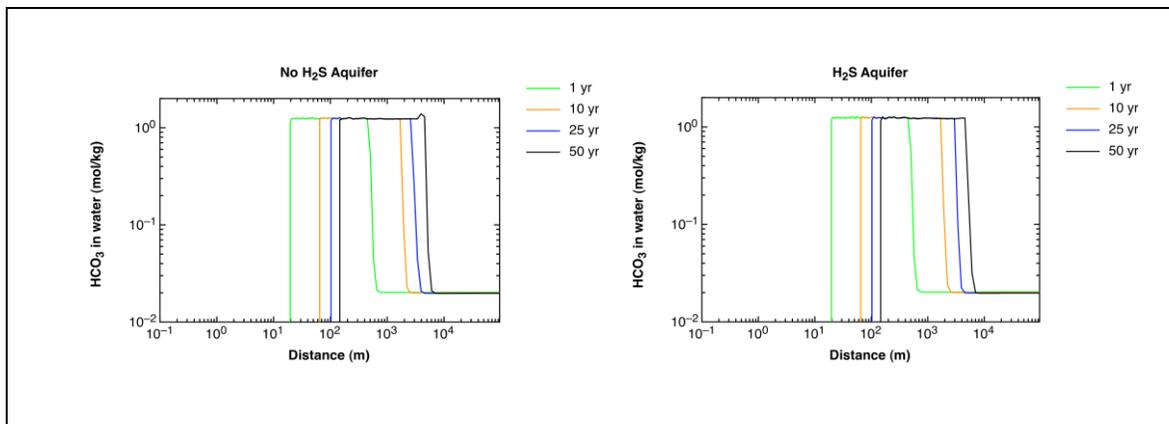

Figure 16: HCO_3 concentration as a function of radial distance after initiation of CO_2 injection for both non-H_2S and H_2S aquifers.

Figures 17 and 18 show the concentrations of calcium and magnesium respectively as a function of distance and time. For calcium the concentration decreased significantly from the initial value of 0.41 moles/kg (red dotted line in Figure 17). Magnesium, however, increased significantly from the initial value of 0.093 moles/kg (red dotted line in Figure 18). The radial trend for the Ca^{2+} and Mg^{2+} concentrations was similar to that of bicarbonate. The concentrations of both species, calcium and magnesium, were zero until 19.2 m for the first year of injection. At this distance, the concentration increased to ~0.02 mol/kg for calcium and ~0.60 mol/kg for magnesium and remained constant to a radial distance of ~570 m. Thereafter, the concentrations decreased and remained constant. This pattern was similar for all years at increasing distances from the injector well (Figures 17 and 18).

Figure 17: Ca concentration as a function of radial distance after initiation of CO_2 injection for both non-H_2S and H_2S aquifers.

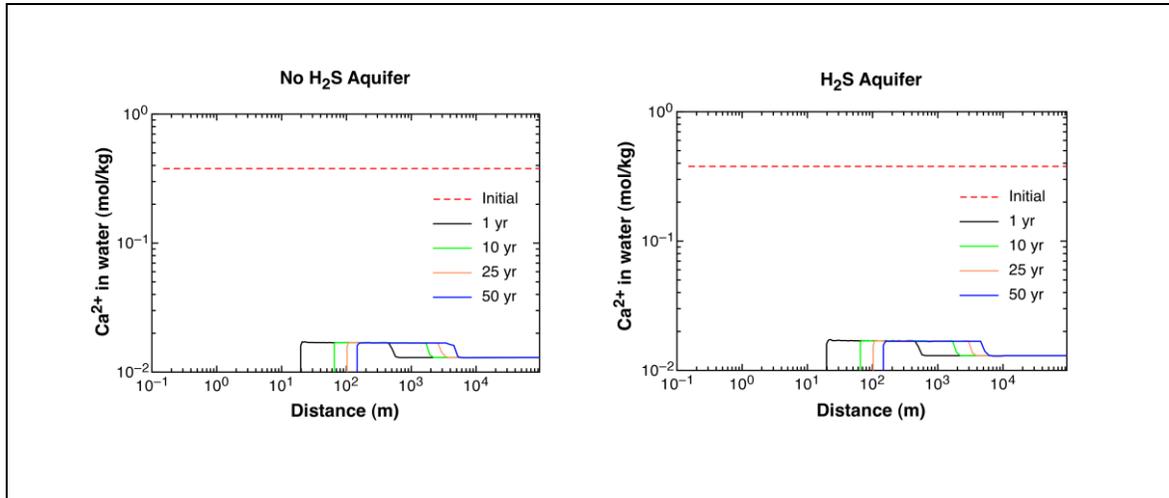**Figure 18**: Mg concentration as a function of radial distance after initiation of CO_2 injection for both non-H_2S and H_2S aquifers.

Figure 19 shows the abundance of dolomite (as a volume fraction) as a function of distance. The initial volume fraction of dolomite (80.49%) decreased by circa 0.4% to a minimum value of 80.10% between 7.8 m and ~500 m. Thereafter, the volume fraction of dolomite increased to ~80.20%. The distance over which the increase in dolomite abundance occurred ranged from ~500 m after one year to ~5200 m after 50 years of injection.

The abundance of calcite as a function of distance and time is shown in Figure 20. Initially the volume fraction of calcite was 0.1604, increasing by 0.36% to 0.1640 between 7.8 and ~500 m, thereafter decreasing to 0.1635. The change in volume fraction was observed up to ~2200 m after 10 years and up to ~5000 m after 50 years.

Figure 19: Dolomite mineral abundance as a function of radial distance after initiation of CO_2 injection for both non-H_2S and H_2S aquifers.
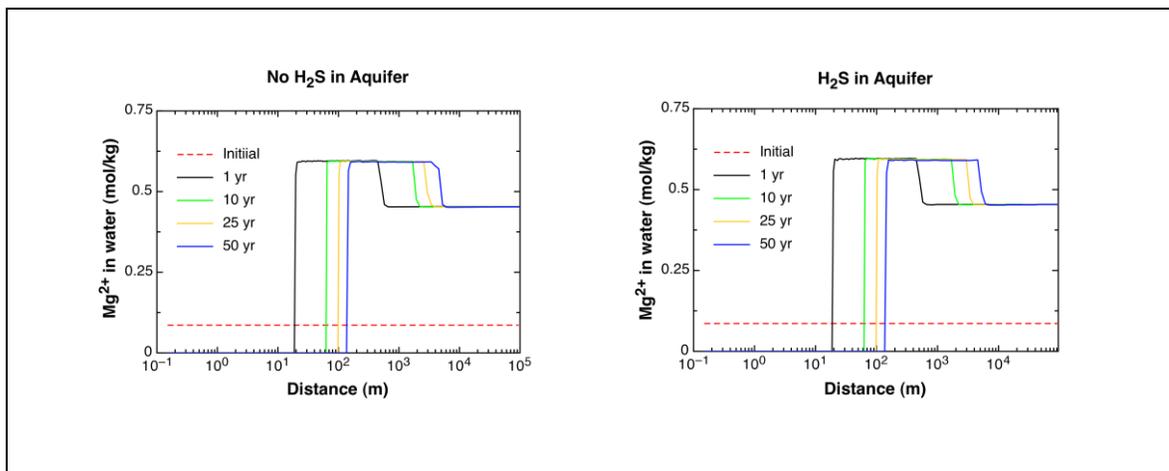

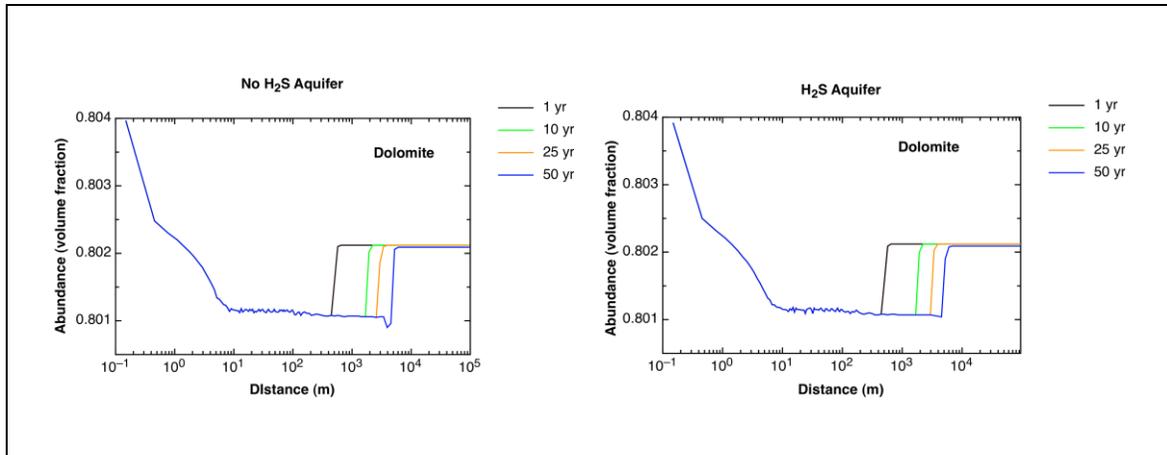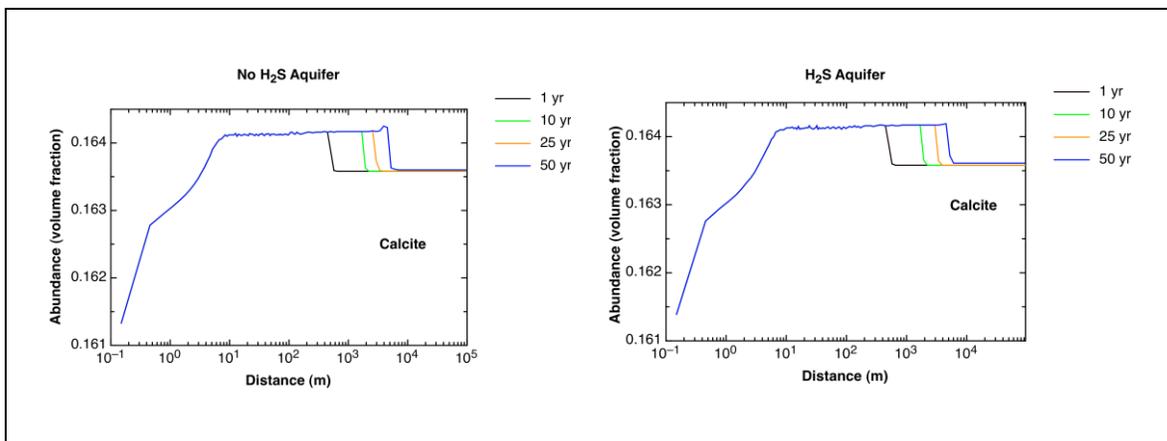**Figure 20**: Calcite mineral abundance as a function of radial distance after initiation of CO_2 injection for both non-H_2S and H_2S aquifers.

Figure 21 shows the changes in the volume fraction of magnesite as a function of distance and time. Initially, there was no magnesite present. After 10 years of injection a small increase in the volume fraction of magnesite on the order of 10^{-5} was observed at a distance of ~1450 m. This small increase persisted throughout the next 50 years without change of the radial distance with almost identical trends for H_2S and no H_2S in the aquifer simulations.

Figure 22 shows the amount of CO_2 sequestered in the mineral phase as a function of both radial distance and time. A decrease in the amount of CO_2 sequestered in mineral form of ~0.36 kg/m^3 was observed at a radial distance of ~500 m after one year of injection indicating that carbonate (dolomite and calcite) dissolution was occurring. The radial distance where carbonate dissolution was occurring increased as injection progressed from ~500 m after one year to ~5200 m after 50 years, and the amount continued to increase slightly to ~0.4 kg/m^3. Outside this dissolution zone, positive CO_2 sequestration values were observed indicating that mineral precipitation is occurring. Mineral sequestration values of ~0.311 kg/m^3 were observed after one year at a radial distance greater than ~500 m and ~0.334 kg/m^3 after 50 years and at a radial distance greater than ~5200 m.

The change in overall porosity as a function of distance and time is shown in Figure 23. After one year of injection, the porosity remained constant at ~10 % within a radial distance of ~570 m. Thereafter the porosity decreased slightly by less than 0.1% to 9.96% for the remaining radial distance. This pattern was similar during the remaining injection period except that the radial distance at which the porosity decrease occurred increased from ~500 m after one year to ~1200 m after five years of injection and ~5200 m after 50 years of injection.
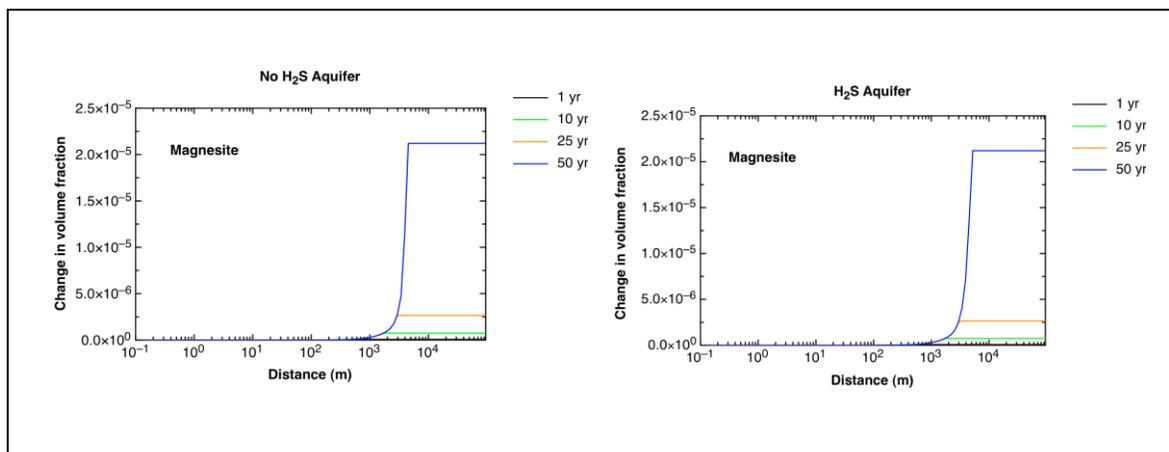
Figure 21: Change in volume fraction of magnesite as a function of radial distance after initiation of CO_2 injection for both non-H_2S and H_2S aquifers.

Figure 22: Amount of CO_2 sequestered in the reservoir in all mineral forms as a function of radial distance after initiation of CO_2 injection for both non-H_2S and H_2S aquifers.
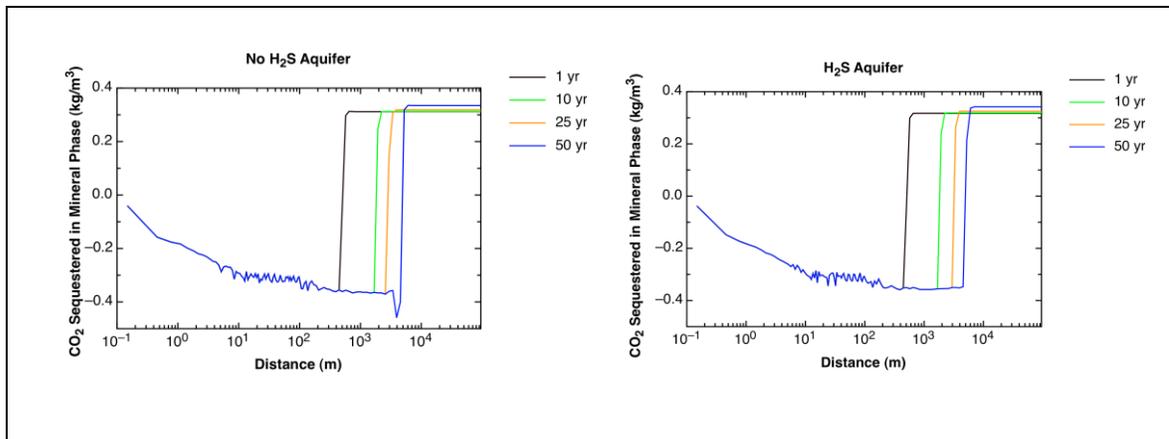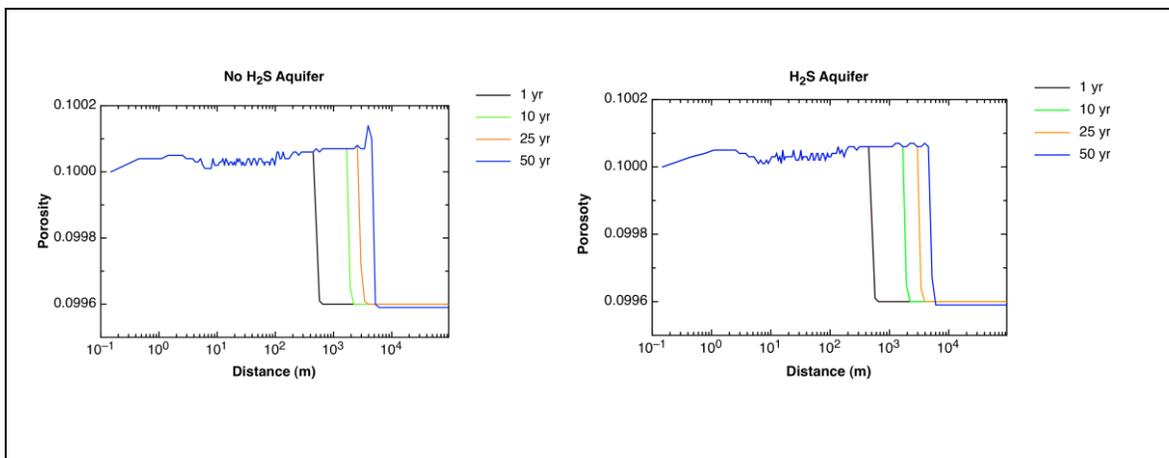

Figure 23: Changes in the porosity of the reservoir as a function of radial distance after initiation of CO_2 injection for both non-H_2S and H_2S aquifers.

3.3.3 Key Findings and Implications

Around the injection well, a region of **complete dehydration** was detected where the value of gas saturation is 1.00. Therefore, no pH values and concentrations of dissolved species are available for this region (Figures 15 to 18). This complete dehydration was probably due to the high rate of injection of dry CO_2, 1MT/yr (31.69 kg/sec). Table 15 summarizes the dehydration region as a function of time ranging from 19.7 m after one year to 136.1 m after 50 years.

Table 15: Injection time of CO_2 and radius of dehydrated region for both H_2S and non-H_2S aquifers.

Time (years)	Radius of the dehydrated region (m)
1.0	19.7
5.0	42.3
10.0	62.3
12.5	67.8
25.0	98.0
37.5	119.6
50.0	136.1

The pH of the initial fluid was 6.1. After one year of CO_2 injection, the reservoir fluid pH decreased to 5.1 within a radius of ~500 m around the injector with a pH increase to 6.4 outside of this region. The lowering of the pH value to 5.1 is caused by CO_2 injection resulting in formation of carbonic acid followed by some dissociation into bicarbonate. The latter results in a significant increase in bicarbonate concentrations in the same region from an initial value of 0.02 moles/kg to 1.25 moles/kg. A similar change in pH and bicarbonate concentrations was evident for all times but at increasing distances from the injector. The increase in bicarbonate concentrations in concert with the decrease in pH indicates that **solubility trapping** was occurring in this region. Table 16 summarizes the amount of CO_2 sequestered in the brine by solubility trapping over the 50-year injection phase. A gradual increase in sequestration of CO_2 over time from 34% to 56% was observed due to the larger fluid volumes available as the CO_2 moves progressively away from the injector into the reservoir.

Table 16: Injection time of CO_2 and amount of CO_2 stored as HCO_3 in the reservoir waters for both H_2S and non-H_2S aquifers.

Time (years)	Amount of CO_2 stored in brine as HCO_3^- (MT)	Percentage of injected CO_2 stored as HCO_3^-
1.0	0.28	34%
5.0	1.66	33%
10.0	3.96	39%
12.5	5.50	44%
25.0	10.8	43%
37.5	17.8	48%
50.0	27.8	56%

A decrease in the concentration of Ca^{2+} (Figure 17) and an increase in the concentration of Mg^{2+} (Figure 18) suggest that dolomite dissolution occurred while calcite precipitated. This was confirmed by dolomite abundances decreasing slightly by 0.3 % (from 80.4 to 80.1 %) due to dissolution within a ~500 m radius around the injector (Figure 19). Calcite showed the opposite trend, i.e., calcite was precipitating over the first ~500 m from an initial volume abundance of 16.1 to 16.4% (Figure 20). Net-carbonate dissolution resulted in minor amounts of ionic trapping. The amount of magnesite formed during the 50-year injection period was negligible, although it represented a new mineral forming in the rock matrix and another potential sink for the injected CO_2 over the longer term.

As CO_2 passed through the reservoir mineral dissolution initially occurred decreasing the amount of dolomite (Figure 19) resulting in more CO_2 released than sequestered. After one year, CO_2 sequestration was observed at a distance >570 m from the injector while this distance increased to ~5200 m after 50 years. The total amount of CO_2 sequestered in the mineral phase after 50 years was 0.334 kg/m^3 at a radial distance of 5200 m. This amount of mineral sequestration is low compared to the amount sequestered in the brine, ~1.25 moles/kg or 8.62 kg/m^3. This indicates that ~26 times more CO_2 is sequestered in the brine compared to mineral trapping. Therefore, the amount of CO_2 sequestration by **mineral trapping** is negligible when compared to the amount of CO_2 sequestered due to solubility and ionic trapping.

The dissolution of dolomite and precipitation of calcite had a very minor effect on the porosity of the reservoir rock, causing a less than 0.1% decrease up to ~570 m after one year of injection and up to ~5200 m after 50 years of injection. While this change in porosity is very small, it is important to evaluate whether precipitation of calcite occurs in the pore or throat region. The latter may negatively impact permeability.

UNIVERSITY OF
CALGARY

Energy &
Environmental
Systems   EES
iseee

4.   SUMMARY

An understanding of the baseline geochemistry of a formation is extremely important in designing a monitoring and modelling program for tracing the fate of injected CO_2 in a saline aquifer (see Lawton et al., this report). Despite the comparatively low number of wells in the Nisku Formation of the study area, a solid understanding of the chemical and isotopic compositions of fluids and gases was obtained by using data from a number of different sources (Section 1). Mineralogical information was compiled using 12 samples from various cores (Section 2). The obtained data were used for geochemical modelling (Section 3) with the goal to assess the fate of CO_2 in the saline aquifer over a 50-year injection period. The key findings of the simplified model runs are as follows:

1. CO_2 injection will likely create a dehydrated region around the injector with a radius increasing from 19.7 m after one year to 136.1 m after 50 years.

2. After one year of CO_2 injection, 34 % of the injected CO_2 will likely be sequestered in the brine as H_2CO_3 and HCO_3^- due to solubility trapping. After 50 years, 56% of the injected CO_2 will likely be sequestered in the brine via solubility trapping.

3. Minor amounts of dolomite are predicted to dissolve and small amounts of calcite will likely precipitate in the reservoir. The extent of ionic and mineral trapping of injected CO_2 will be, however, small compared to solubility trapping in the saline aquifer. According to the simplified model approximately 26 times more CO_2 will be sequestered in the brine via solubility trapping as compared to mineral trapping.

4. There were no significant observable differences in the chemical or mineralogical reactions between the H_2S and non-H_2S containing saline aquifers.

5. The porosity of the reservoir rocks will likely decrease in the CO_2 injection zone by less than 0.1%. It was impossible to assess the impact of the porosity change on permeability within the scope of this study.

REFERENCES

[1] Schrag, D.P., 2007, Preparing to capture carbon. Science. 315. No. 5813, 812.

[2] Raistrick, M., Mayer, B., Shevalier, M., Perez, R., Hutcheon, I., Perkins, E., and Gunter, B., 2006, Using chemical and isotopic data to quantify ionic trapping of injected carbon dioxide in oil field brines, Environmental Science and Technology, 40:6744-6749.

[3] S. Emberley, S., Hutcheon, I., Shevalier, M., Durocher, K., Gunter, W.D., and E.H. Perkins, E.H. (2005), Geochemical monitoring of fluid-rock interaction and CO_2 storage at the Weyburn CO_2-injection enhanced oil recovery site, Saskatchewan, Canada. Applied Geochemistry, 29:1393-1401.

[4] Gunter, W.D., and E.H. Perkins, E.H., and Hutcheon, I.E., 2000, Aquifer disposal of acid gases: modelling of water-rock reactions for trapping of acid wastes. Applied Geochemistry, 15:1085-1095.

[5] Simpson, G., 1999, Sulfate reduction and fluid chemistry of the Devonian Leduc and Nisku formations in south-central Alberta. Ph.D. Thesis, University of Calgary (unpublished).

[6] Bachu, S., Sauveplane, C.M., Lytviak, A.T., Hitchon, B., 1987, Analysis of Fuid and heat regimes in sedimentary basins: techniques for use with large data bases. American Association of Petroleum Geology Bulletin, 71:822–843.

[7] de Caritat, P., Bloch, J., and Hutcheon, I., 1994. LPNORM: A linear programming normative analysis code; Computers and Geosciences, v. 20, p. 313-347.

[8] Carpenter, S. J., and Lohmann, K. C. d18O and d13C variations in Late Devonian marine cements from the Golden Spike and Nevis Reefs, Alberta, Canada: Journal of Sedimentary Petrology, v. 59, (1989) p. 792-814.

[9] Whittaker, S. G. and Mountjoy, E. W. Diagenesis of an Upper Devonian Carbonate-Evaporite Sequence: Birdbear Formation, Southern Interior Plains, Canada Journal of Sedimentary Research, Section A: Sedimentary Petrology and Processes   Vol. 66 (1996) No. 5. (September), Pages 965-975

[10] Machel, H.G. (1985) Facies and diagenesis of the Upper Devonian Nisku Formation in the subsurface of central Alberta. Ph.D. Thesis, McGill University, Montreal, 392.

[11] Kharaka, Y. K., Gunter, W., Aggarwal, P. K., Perkins, E. H. and De Braal, J. D., 1988. SOLMINEQ88: a computer programme for geochemical modelling of water-rock reactions. *USGS Water Resources Investigation Report,* 88-4227.

[12] Alberta Geological Survey, 2005, Test Case for Comparative Modelling of CO_2 Injection, Migration and Possible Leakage - Wabamun Lake Area, Alberta, Canada, Alberta Geological Survey Website, http://www.ags.gov.ab.ca/co2_h2s/wabamun/Wabamun_base.html

[13] Duan, Z., Sun, R., and Zhu, C., 2007, Accurate thermodynamic model for the calculation of H_2S solubility in pure water and brines, Energy and Fuels, 21:2056-2065.

[14] Xu, T., Pruess, K., and Brimhall, G., 1999, An improved equilibrium-kinetics speciation algorithm for redox reactions in variably saturated subsurface flow systems. Computers and Geoscience, 25:655-666.

[15] Xu, T., Apps, J., and Pruess, K., 2004, Numerical simulation of CO_2 disposal by mineral trapping in deep aquifers. Applied Geochemistry, 19:917-936.

[16] Weir, G.J., White, S.P., Kissling, W.M., 1995. Reservoir storage and containment of Greenhouse gases. In: Pruess, K. (ed.), Proceedings of the Tough Workshop '95. Lawrence Berkeley National Laboratory Report LBL-37200, pp. 223-238. Berkeley, California.

[17] Ennis-King, J. and Patterson, L., 2003. Role of convective mixing of the long term storage of carbon dioxide in deep saline formations. Paper SPE 84344, Presented at Society of Petroleum Engineers Annual Fall Technical Conference and Exhibition, Denver CO, October 2003.

[18] Van Genuchten, M.Th., 1980, A closed-form equation for predicting the hydraulic conductivity of unsaturated soils. Soil Sci. Soc. Am. J., 44, 892–898.

[19] Corey, A.T., 1954, The interrelation between gas and oil relative permeabilities. *Prod. Mon.* 38–41.

[20] Palandri, J., Kharaka, Y.K., 2004*, A compilation of rate parameters of water–mineral interaction kinetics for application to geochemical modelling.* US Geol. Surv. Open File Report 2004-1068.64.

[21] Xu, T., Apps, J., Pruess, K., Yamamoto, H., 2007, Numerical modelling of injection and mineral trapping of CO_2 with H_2S and SO_2 in a sandstone formation, Chem. Geol., 242,i 319–346.